The Effect of Sabot Grooves on Lift Force for Kinetic Energy Projectiles

Ameer G. Mikhail

19990325 058

Approved for public release; distribution is unlimited.

Abstract

The effect of grooves on the normal force of an anti-armor long rod kinetic energy (KE) projectile was analyzed and numerically quantified. The effect was studied for body alone and body with fins in which clear and distinct effects were experimentally observed for each. Wind tunnel data sets were analyzed, and algebraic, semi-empirical correlations were constructed using the main physical parameters of the projectile body and fins, as well as the flow parameters. The correlations provide a simple method of estimating the increase or decrease in the vehicle's total normal force attributable to grooves and can be implemented in fast aerodynamics design codes. One separate set of data was dedicated for independent validation, and the correlation predicted the effect reasonably well, both in magnitude and sign. The present correlation is the only one known in the literature for predicting the lift loss (or gain) attributable to grooves. In addition, a better understanding of the contributions of grooves to both body alone and fins in the presence of a body is presented. The correlation is constructed for the Mach number range of $2.0 < M < 5.5$ and for small angles of attack (less than $6°$), which cover the flight envelope of tactical KE anti-armor projectiles. The established correlations provide direct incremental lift coefficient corrections over smooth body values for useful direct design use.

TABLE OF CONTENTS

INTENTIONALLY LEFT BLANK

LIST OF FIGURES

INTENTIONALLY LEFT BLANK

LIST OF TABLES

INTENTIONALLY LEFT BLANK

THE EFFECT OF SABOT GROOVES ON LIFT FORCE FOR KINETIC ENERGY PROJECTILES

1. INTRODUCTION

In many instances in the design and testing of anti-armor kinetic energy (KE) projectiles, as the one depicted in Figure 1, the fin effectiveness in providing the normal force for stability and pitch damping is questioned because of the nonquantified effect of the rod body's grooves. These grooves are needed to transmit the launching force from the driving sabot. As for any other unknown parameter, this effect is usually either minimized or exaggerated. No tool that can predict this usually small effect exists. In fact, it is generally not known if the grooves will increase or decrease the total vehicle lift force. Although the effect is generally acknowledged as small, one needs a fast prediction method to estimate the magnitude and the sign of the expected change in the normal force. This need is the motivating force behind the present work. The physical phenomenon of the groove-boundary layer interaction on the body and along the fin-body junction is not very simple and does not lend itself easily to fast prediction methods. The practical approach of relying on actual force measurements data and translating them into empirically formulated expressions seems appealing and more practical. In fact, the same approach was also used a decade earlier by Mikhail[1] in studying the effect of the grooves on the drag force. The grooves effect on the drag force is more pronounced than that on the lift force. Although empirical, those drag correlations were applied by other researchers[2] and were found to be very useful and more accurate[2] than other estimates.

The available data are relatively sparse but sufficient to construct a correlation. Khan and Chung[3] conducted wind tunnel tests of body alone with and without grooves. Brandon and von Wahlde[4] performed large scale wind tunnel tests of KE projectiles, including body alone and body with fins. Sigal[5] tested body alone and body with fins and flare in wind tunnel but for limited Mach numbers. Fellows[6] performed wind tunnel tests for body with fms, which were later also reported by Hendry[7].

Range tests were also performed on some limited configurations.[2,8] Since the groove effects are usually small, they normally fall close to the measurement accuracy of the normal force. In Reference 8, few measuring stations were used and CN_α could not be reliably reduced from the data. Thus, no reliable values were available from free-flight range tests for grooved versus smooth models. Also, another range test was performed[9], with the same outcome regarding the uncertainty of the normal force slope coefficient measurements. Hopefully, future firings may be aimed at obtaining more confirmed measurements.

The boundary layer over the grooved body at the Mach number range of interest (2 to 5) is always turbulent, except maybe over the nose tip section. For body alone, the grooves seem to increase the pressure difference between the windward and leeward sides, causing an increase in the lift force. For finned bodies, the exact mechanisms affecting the fins are not very well explained. However, explanations are usually proposed that the grooves may increase the boundary layer thickness or cause flow unsteadiness over the fins.

More recently, turbulent boundary layer measurements were made[10] at Mach = 5 and zero angle of attack for a flared body. Large grooves of square profiles of depths of 5 mm (0.2 inch) and 10 mm (0.4 inch) (2.54 and 1.27 grooves per inch, respectively) and 45" sawtooth grooves were tested. Surface pressure, turbulent boundary layer parameters, and heat flux measurements were reported. Because of the large groove pitch and depth, each single groove acts as a single cavity where the flow impacts the facing surface of the circumferential cylindrical cavity. Only flow variables (no forces) were reported at the zero angle of attack tests. The surface pressure was then integrated to estimate the forebody drag coefficient.

2. ANALYSIS

The effect of the grooves on the normal force is modeled as a correction factor to the normal force coefficient for the smooth body value. Since we are usually dealing with small a, the lift force will be interchanged with the normal force without loss in meaning ($CN = CL \cos \alpha + CD \sin a$, and for small a, $CN \approx CL$). First, the normal force coefficient for the body-fin combination is usually written as

$$CN_{\alpha,bf} = CN_{\alpha,b} + \left(K_{w(b)} + K_{b(w)} \right) CN_{\alpha,ff} \qquad (1)$$

$$\equiv CN_{\alpha,b} + CN_{\alpha,f} \qquad (2)$$

in which $CN_{\alpha,ff}$ is the pure fin-alone normal force coefficient, with no body attached to it. Now, for the body alone, we introduce the definition of F_b as

$$F_b = \frac{\Delta CN_{\alpha,b}}{CN_{\alpha,bs}} \equiv \frac{\left(CN_{\alpha,bg} - CN_{\alpha,bs} \right)}{CN_{\alpha,bs}} \qquad (3)$$

For body with fins, we introduce the factor F_{bf} as

$$F_{bf} = \frac{\Delta CN_{\alpha,bf}}{CN_{\alpha,bf,s}} \equiv \frac{\left(CN_{\alpha,b} - CN_{\alpha,f}\right)_g - \left(CN_{\alpha,b} + CN_{\alpha,f}\right)_s}{\left(CN_{\alpha,b} + CN_{\alpha,f}\right)_s} \tag{4}$$

The correction for the groove effect on the fin (in the presence of a body) can be deduced when we define F_f as

$$F_f = \frac{\Delta CN_{\alpha,f}}{CN_{\alpha,bf,s}} \equiv \frac{\left(CN_{\alpha,fg} - CN_{\alpha,fs}\right)}{\left(CN_{\alpha,b} + CN_{\alpha,f}\right)_s} \tag{5}$$

Therefore, since tests for body groove effects on fin lift can only be made in the presence of bodies, the pure fm alone is not applicable. However, the effect of grooves on fin lift (in the presence of a body), F_f, can be deduced from both F_b and F_{bf}, after simple algebraic simplification   as

$$F_{bf} = F_b \left(\frac{\left(CN_{\alpha,b}\right)_s}{\left(CN_{\alpha,b} + CN_{\alpha,f}\right)_s} \right) + F_f \tag{6}$$

thus

$$F_f = F_{bf} - F_b \left(\frac{\left(CN_{\alpha,b}\right)_s}{\left(CN_{\alpha,b} + CN_{\alpha,f}\right)_s} \right) \tag{7}$$

Therefore, the effort in this work is to determine the values of F_b and F_{bf} from the test data and then deduce F_f. The user for any application can then use the computed values of F_b, F_f, and F_{bf} to compute $\Delta CN_{\alpha,bg}$, $\Delta CN_{\alpha,fg}$, and $\Delta CN_{\alpha,bf,g}$, based on the smooth-body values of $CN_{\alpha,bs}$, $CN_{\alpha,fs}$, and $CN_{\alpha,bfs}$. Note that the definitions of $F's$ are presented as fractions of the change in groove lift (increase or decrease) relative to the lift value of the smooth body.

The value of F_b, F_f, or F_{bf} is usually less than 0.15, indicating a 15% maximum change over the corresponding smooth-body value. As will be shown later, F_b is always positive and F_f is always negative, resulting in F_{bf} being either positive or negative, as implied in Equation (6).

For most KE projectiles, the grooves are manufactured with a standard pitch-to-height ratio. Therefore, either the pitch or the groove depth may be specified. For practical aspects, the groove pitch is more visible and easily identified. So, in the present work, only the groove pitch is reflected in the correlations. Considerably deep, nonstandard grooves may then require different considerations.

It is reported[3-5] that the position of center of pressure for the body alone and body with fins will also be slightly affected by the grooves. However, a separate study may be dedicated to investigate the exact trend and magnitude. The present work does not include this aspect. However, from the available published data, it seems that for body alone, the center of pressure moves slightly backward, away from the nose. For bodies with fins, the loss in fin lift will cause a slight forward movement toward the nose. Thus, for the combined body and fins, the final shift can be forward or backward, depending on the relative contributions of the changes attributable to body alone and to the fins.

The developed correlation formulae are written in the form of multiple factors. Each factor is dimensionless, generally on the order of O(l), and each reflects specific physical parameters or geometrical features of the configuration. This approach proved successful in the earlier study of Reference 1. The expressions are then developed based on selecting the dominant variables that are identified to be most influential, based on basic aerodynamic considerations and on the several data sets that were examined. Simple algebraic variations are used when no theory is available, such as for the effect of the groove pitch. The constants in the formulae were then determined after several fitting iterations, so that the results for all the cases can be reproduced to a satisfactory accuracy with one set of constants.

2.1 Body Alone

The body-alone, normal force, groove-correction increment was identified to be affected by the nose shape, nose length, grooved body length, groove starting distance from the nose end, groove pitch, Mach and Reynolds numbers. The associated symbols and nomenclature used are defined in Figure 2.

The nose shape factor, F_1, represents the two parameters of the nose shape and length. The first parameter reflects the ratio of a conical nose slope to the average slope of each of possibly two different nose sections. The total body-length-to-nose-length ratio is reflected in the second parameter. F_2 reflects the nose-body junction step effect which was observed from the data of Reference 3. Note that this effect is also tied to the location of the start of the grooving on the body. For a continuous nose-body junction, this factor reduces to a value of 1 .O. Both factors F_3 and F_4 reflect the groove pitch and total length of groove effects that were found to be coupled and not purely independent. Two different; separate groove lengths with different groove pitches are allowed. The groove lengths are tied to the body cylindrical length, L_c, instead of the total body length in order to exclude the nose length which does not influence these two factors. F_5 provides a factor reflecting the reduced lift loss with the increase in both Mach number and unit Reynolds

number. The following form was then assembled, based on these basic factors and their contributions. This particular form was also guided by all the data[3-5] examined.

$$\frac{\Delta CN_{\alpha,b}}{CN_{\alpha,bs}} = F_b = +0.015 [F_1 F_2 F_3 F_4 F_5] \tag{8}$$

in which

$$F_1 = \left| \left(\frac{l_n tan^{-1} \left\{ \frac{d_{nb}}{l_n} \right\}}{l_{n1} \tau_1 + l_{n2} \tau_2} \right)^{2.0} \left(1.+ 0.1 \left| \frac{L_t}{l_n} \right\}^{0.5} \right) \right|,$$

$$F_2 = \left[1.+15. \left(\frac{d_{nb} - d}{d} \right) (1.+ 20. \ tan\{\delta_{nb}\}) \left(\frac{1.-l_{bg}}{L_c} \right)^0 \right],$$

$$F_3 = \left[1.165 (1.-e^{-0.5 l_g / d}) \left(1.+ 0.15 \left\{ \frac{l_g}{d} \right\}^{0.4} \right) \left(\frac{1.- l_{bg}}{L_c} \right) \right],$$

$$F_4 = \left[1.+0.28 \left(\left\{ \frac{p_1}{0.031} \right\}^{0.7} \left\{ \frac{l_{g1}}{L_c} \right\} + \left\{ \frac{p_2}{0.031} \right\}^{0.7} \left\{ \frac{l_{g2}}{L_c} \right\} \right) \right],$$

$$F_5 = \left[\left(0.5+0.5 \sqrt{\left\{ \frac{1.4 x 10^6}{Re} \right\}} \right) \left(\frac{4.0}{M_\infty} \right)^{0.2} \right],$$

$$l_g = l_{g1} + l_{g2},$$

in which p_1 and p_2 are the groove pitches in inches and τ_1 and τ_2 are the average cone half angles (in radians) for the first and second nose sections, if applicable. For a continuous nose surface, τ_1 and τ_2 represent the average nose slope angles at 1/3 and 2/3 of the nose length.

2.2 Fin in the Presence of a Body

To formulate a correlation for F_f, the numerical data values from experiments had to be deduced from those of the total vehicle value represented by F_{bf} and then the body-alone contribution, F_b, had to be subtracted, as governed by Equation (7), to get F_f. The values for the F_f and their trends were then used to guide the development of the correlation. The associated nomenclature is defined and depicted in Figure 2.

The main influencing parameters were identified as the fm aspect and taper ratios, number and orientation of fins, grooved body length and groove pitch, distance between the end of the grooves and the beginning of the fin root, and both the Mach and Reynolds numbers (reflecting the boundary

layer height at the fin). As before, the multiple factors form is constructed, reflecting those parameters. The factor G_1 reflects the effect of the boundary layer thickness to fin semi-span ratio, the root chord length and the taper ratio, and the total number of tins. The length of the grooves and their pitch are represented by G_2 and G_3, which allow for two different types and lengths of grooves. Note that the location (distance from the grooves' end to the fin) and the starting distance from the nose for the grooves do not seem to have an effect on the fin loss. Also, the fm thickness does not seem to be a significant factor in the lift loss; therefore, it was not included. G_4 reflects the Mach and Reynolds numbers and adjusts for the flat plate boundary layer value. The G_5 factor, reflecting the fm roll angle orientation effect, is discussed later. Finally, the following form was assembled, guided by the numerical values deduced from all the data[4-5] examined.

$$\frac{\Delta CN_{\alpha,f}}{CN_{\alpha,bf,s}} = F_f = -0.09 [\, G_1 G_2 G_3 G_4 G_5 \,] \tag{9}$$

in which

$$G_1 = \left[\left(\frac{\delta}{0.5b} \right) \left(\frac{C_{cont}\{1.+Tr\}}{\{d+0.5b\}} \right) \sqrt{N/4} \, \right],$$

$$G_2 = \left[1.+ 0.1 \left(\left\{ \frac{p_1}{0.031} \right\}^{0.8} \frac{l_{g1}}{L_f} + \left\{ \frac{p_2}{0.031} \right\}^{0.8} \frac{l_{g2}}{L_f} \right) \right],$$

$$G_3 = \left[1.+ 0.15 \left(\left\{ \frac{p_1}{0.031} \right\}^{n1} \frac{l_{g1}}{L_f} + \left\{ \frac{p_2}{0.031} \right\}^{n2} \frac{l_{g2}}{L_f} \right) - \left(1.4 \frac{l_{eg}}{L_f} \right) \right],$$

$$G_4 = \left[\sqrt{\left(\frac{Re}{(5.0 \times 10^6)} \right)} \left(\frac{1}{M_\infty^{0.65}} \right) \right],$$

$$G_5 = [G_{orien}],$$

$$\delta = \left[0.5 \; C_{f\infty} \; Xf \left(\frac{0.558}{\sqrt{c_f}\left\{ 1.- \frac{2\sqrt{c_f}}{0.558} \right\}} \right) \right],$$

$$c_f = \frac{0.558 \; C_{f\infty}}{0.558 + 2.0\sqrt{C_{f\infty}}}, \frac{0.242}{C_{f\infty}} = log_{10}\left(R_\infty \, C_{f\infty} \right),$$

$$n1 = 1.- 0.08\left(\frac{p_1}{0.031} \right), \; n2 = 1.- 0.08\left(\frac{p_2}{0.031} \right),$$

in which N is the number of fins, δ is the compressible, turbulent, flat plate boundary layer thickness[11] estimated at the fin's most forward point of the root chord, x_f, Tr is the fin taper ratio ($= C_{tip}/C_{root}$), and R_∞ is the Reynolds number based on the total projectile length.

2.2.1 *Fin Roll Orientation Model*

The roll orientation effect of the fins was reported[5] in a wind tunnel test for four-finned configurations. The effect was large for that configuration but is expected to be smaller for six-finned or N-finned bodies because of the smaller angular interval. The orientation factor was constructed, based on the data of Reference 5 for four fins at two roll angles. It is also constructed to yield the value of 1 .0 for a six-finned configuration at zero roll angle. The orientation factor, in association with G_5 of Equation (9), is formed as

$$G_{orien} = \frac{\left[N_{aff}\left(N_i cos^2\left\{ \frac{\pi}{N} - k \right\}\right)\right]}{\left[N \sum_{i=1}^{N} cos^2(\phi_i)\right]} \tag{10}$$

in which

N_{aff} = N-l .-cos(N Φ)

Φ = configuration roll angle measured from the vertical plane ($\Phi = 0$ when a fm is aligned directly up in the vertical plane)

ϕ_i = individual tin panel angle plane with respect to the horizontal plane

N_i $= N_{aff}$ for $N = 4$

             $= N$ for $N \neq 4$

k $= \pi/2$ for $N = 2$

             $= 0$ for $N \neq 2$

For a four-finned projectile at 45" roll, the G_{orien} is 1 .O, while it is only 0.25 for 0" roll. For a six-finned vehicle with one fin aligned with the vertical plane ($\Phi = O.O$), $G_{orien} = 1 .O$ and it equals 1.5 when the roll angle Φ is 15°. Therefore, the fm roll orientation has a relatively large effect on the fin lift loss because of the grooves. This effect is also more pronounced for the four-finned than for the six-finned configurations.

2.3 Body With Fins

Let us define the grooved correction factor for a body with fins. The smooth-body normal force slope coefficient component build-up for a wing with no cant (deflection) angle is usually written as (Eq. 1)

7

$$CN_{\alpha,bf,s} = CN_{\alpha,b,s} + \left(K_{w(b)} + K_{b(w)}\right)CN_{\alpha,ff,s}$$

Now, for a grooved body, the present analysis for the correction expression is written as

$$CN_{\alpha,bf,g} = CN_{\alpha,b,s}\left(1.+F_b\right) + \left(K_{w(b)} + K_{b(w)}\right)\left(1.+F_f\right)CN_{\alpha,ff,s} \qquad (11)$$

One might note that the $(1.+F_f)$ factor appears outside both $K_{w(b)}$ and $K_{b(w)}$ because the F_f **was** deduced by subtracting the body-alone normal force from the "total vehicle" value; thus, the effect of the $K_{b(w)}$ could not be separated from $K_{w(b)}$. Therefore, for a body with fins, from Equations (4) and (6),

$$\frac{\Delta CN_{\alpha,bf}}{CN_{\alpha,bf,s}} = F_{bf} = F_b\left(\frac{\left(CN_{\alpha,b}\right)_s}{\left(CN_{\alpha,b} + CN_{\alpha,f}\right)_s}\right) + F_f. \qquad (12)$$

2.4 Body With Flare

For flared bodies, some limited data exist for body alone and body with flare[5]. The present analysis concerns the flare as if it were "fins"; thus, one can easily establish

$$F_{bfl} = F_b\left(\frac{\left(CN_{\alpha,b}\right)_s}{\left(CN_{\alpha,bfl}\right)_s}\right) + F_{fl}. \qquad (13)$$

To obtain the flare-in-the-presence-of-a-body factor, F_{fl}, the body-alone contribution has to be subtracted from the total vehicle (body and flare) value, as was done in the finned body case. The body alone is extended to the end of the flare base. From Equation (13), one obtains

$$F_{fl} = F_{bfl} - F_b\left[\frac{\left(CN_{\alpha,b}\right)}{\left(CN_{\alpha,bfl}\right)_s}\right].$$

The main parameters affecting the lift loss are represented by the flare geometry, the groove length and pitch, and both the Mach and Reynolds numbers. The multiple factors form was also used. The first factor, H_1, reflects the flare base diameter and cone half angle. The factor H_2 reflects the groove length and pitch. The factor H_3 reflects the Mach and Reynolds number effects. The experimentally deduced values for F_{fl} were then fitted into the following correlation:

$$\frac{\Delta CN_{\alpha,fl}}{CN_{\alpha,bfl,s}} = F_{fl} = +0.35\left[H_1 H_2 H_3\right] \tag{14}$$

in which

$$\Delta CN_{\alpha,fl} = \left(CN_{\alpha,fl,g} - CN_{\alpha,fl,s}\right).$$

As in the fin case, F_{fl} is not purely flare-alone value but is flare in the presence of a body. Its definition is purely mathematical, to be consistent with the body-alone and the total vehicle (body and flare) definitions. Its value is not measured directly but rather is deduced by subtracting the body-alone value from the total vehicle value.

The following forms for the different H factors of Equation (14) were formulated, reflecting the previous considerations and with the different constants being guided by the data set of Reference 5. The associated nomenclature is also defined in Figure 2.

$$H_1 = \left[\left(\frac{d_f}{d}\right)\left(\frac{d_f - d}{2l_f}\right)\right],$$

$$H_2 = \left[0.3 + 0.25\left(\left\{\frac{p_1}{0.031}\right\}^{m1}\left\{\frac{l_{g1}}{L_f}\right\}\left\{\frac{p_1}{0.157}\right\}^{0.5} + \left\{\frac{p_2}{0.031}\right\}^{m2}\left\{\frac{l_{g2}}{L_f}\right\}\left\{\frac{p_2}{0.157}\right\}^{0.5}\right)\right],$$

$$m1 = 1.- \ 0.05\left[\_\_0.03\,p_1 \ \ \ \ m2 = 1.\_0.05\right[\_\_\_\_ p_2 \right],$$

$$H_3 = \left[\left(0.5 + 0.5\sqrt{\left\{\frac{1.4 \times 10^6}{Re}\right\}}\right)\left(\frac{1.}{M^{0.1}}\right)\right]$$

2.5 Applying the Correlations

Equations 8, 9, 12, and 14 provide the incremental change in normal force slope coefficient attributable to grooves, ACN, as a fraction of the corresponding smooth-body value. This groove correction is then added to correct the estimated normal force for the smooth-body vehicle.

Since the present correlations are based on test data, they are expected to provide best results when applied within the ranges of the parameters used. This means a Mach range between 2 and 5.5, small angles of attack to 6°, and fin aspect ratios of 0.3 to 2.0. Results obtained by applying the correlations in extrapolated regions beyond these limits should be well examined. In addition, the flare correlation was based on limited data and thus is expected to be less versatile.

3. ABOUT THE DATA USED

3.1 Data of Khan and Chung

These data only concern body alone. Four long bodies with slightly different nose shapes were tested in a "blow-down" wind tunnel at Mach 4. In addition to the smooth-body model, two different groove lengths were tested for each nose shape. The groove lengths are 3.9 and 18.5 calibers, and they both begin immediately after the nose section. All models had a length-to-diameter (L/d) ratio of about 2 1.8, with a model diameter of 19.46 mm (0.717 inch). Three series of body models were tested. Model series 1000 has the grooves over the total cylindrical body length for four nose types (models 1100, 1200, 1400, and 1500). Model series 2000 has grooves over only the first 3.9 calibers of the body for the same four nose types (models 2 100, 2200, 2400, and 2500). Model series 4000 has no grooves at all on the cylindrical body for the same four nose types (models 4100, 4200, 4400, and 4500). Model 1100 had a $10°$ semi-vertex cone nose followed by short cylindrical section. Model 1200 had a $10°$ semi-vertex cone followed by a short, 3" half-angle frustum. Model 1400 had two shorter conical nose sections of half angles of 22" and $10°$, respectively, followed by a short cylindrical section. Model 1500 had a Sears-Haack ogive nose. The test Reynolds number was about 1.4×10^6 per foot. The thread types are 0.759-inch-32UNS-2A (0.759-inch mean diameter and 32 threads per inch).

3.2 Data of Brandon and von Wahlde

This set of data is large and encompasses body alone and body with fins. Both configurations were tested with smooth and grooved bodies. Tests were made at Mach 3.5, 4.0, and 5.0. Bodies with L/d ratios of 20.6, 25.6, 30.6, and 35.6 were tested. The body diameter was 0.94 inch (23.98 mm), and the Reynolds number per foot varied between 4.0×10^6 and 5.6×10^6. The grooved models have two sections with different types of grooves to test the effect of groove types. The notation G/S, G/T, G/G represents front/rear body groove types (S = smooth body, T = threads of 32 threads per inch, G = grooves of eight grooves per inch). Most of the groove effect tests were made with a shortened length of a Sears-Haack nose ogive. For finned configurations, only one set of fins (six fins) was tested at one roll angle setting (zero roll). Tests were made between $\alpha = \pm 4°$. Test results were questionable for some runs because of the fast continuous a sweep measurements and the total length of the projectile. Models were sting mounted, causing some bending of the long rods and resulting in asymmetrical CN_α variation with positive and negative a. The tabulated data in that reference were checked versus the plotted results when the tabulated value was suspected. The report stated that because of this asymmetry, data points for CN were "averaged" over the negative and positive a, thus contaminating the correct value. Some results were limited between $\alpha = \pm 2°$

instead of ±4°. In some cases, the negative a sweep points were neglected altogether. In the present study, some suspect values were tracked and corrected from their plotted values in the given reference. The test model for this set of data is depicted in Figure 3.

3.3 Data of Sieal

This set of data was generated for Mach numbers 0.8 and 2.4 only. Only the supersonic speed data were analyzed and used in the present work, since the speed range for the KE projectiles is usually between M = 5 and M = 2. The tests were run for a between ±5° at Reynolds number of 25.9×10^6 per foot. The diameter of the test model is 40 mm (1.57 inches) and the total length is 13.5 calibers. The ogive nose length is 3.5 calibers, and the grooved section is 8 calibers long and begins at the end of the nose section. Four types of surface roughness and grooves were tested in addition to the smooth body. All surface grooves and roughnesses have a height of 0.5 mm (0.02 in.), and all grooves had sharp rectangular profiles. The first type is a knurled surface roughness while the second has 25.4 threads per inch. The third type has 12.7 grooves per inch, and the fourth type has 6.35 grooves per inch. For the finned configuration, four trapezoidal fins with an aspect ratio of 1.35 and taper ratio of 0.3 were used. The configuration was tested in the + and x (i.e., 45" roll) formations. For the flared configuration, a frustum conical flare length of 2 calibers and semi-cone angle of 7.1 ° was used. No estimates for the error in measurements were given.

3.4 Data of Fellows-Carberry and Hendry

The data of Reference 6 are only for a body with fins, at Mach numbers of 2.0, 3.0, 4.0, and 4.9. The data were summarized and reported later in Reference 7. The configuration had six trapezoidal fins that had a taper ratio of 0.45 and an aspect ratio of 0.37. The tests were made at zero roll angle (one fin aligned with the vertical plane). The test model had an L/d ratio of 16.1 and diameter of 44 mm (1.73 in). Three patterns of groove lengths were tested, including a large single length, two smaller unconnected lengths, and a small central length. Only the two unconnected lengths case provided consistent behavior. The grooving is eight grooves per inch. The test model for these data is shown in Figure 4.

This set of data was not purposefully included in deriving the correlations, since an independent test was needed after the correlations were constructed to examine its prediction. This set was chosen because it has the unique feature of two separated grooved sections and

because the data showed larger scatter. These features would test the correlations in a harsher, non-typical case.

3.5 Error Estimation for Values Deduced From Experiments

Although the error in measurements in $CN_{\alpha,s}$ and $CN_{\alpha,g}$ might be small, the error in their relative differences represented by $\Delta CN_\alpha/CN_{\alpha s}$ is quite large, as exemplified by the following example. Let the measurement errors in $CN_{\alpha s}$ and $CN_{\alpha g}$ be ±3%, with measured values of 4.7 and 5.0 per radian, respectively. The direct value for $\Delta CN_\alpha/CN_{\alpha s}$ would be +6.38%, while the highest and lowest possible values would be +12.96% and +0.18%, respectively. This indicates an error of +103% or -97% in the $\Delta CN_\alpha/CN_{\alpha s}$ value. Therefore, although the measurements of CN_α are within ±3%, the corresponding error in the deduced $\Delta CN_\alpha/CN_{\alpha s}$ is ±100%. In the present work, the experimentally deduced values for $\Delta CN_\alpha/CN_{\alpha s}$ will be considered having an error bound of ±100%. So, if the experimental F_{bf} value is -0.03, this indicates a normal force slope coefficient decrease in the range of 0.0% to -6.0%.

4. **RESULTS**

'Listings of the physical parameters and the computed results for body alone, body with flare, and body with fins are given in Tables 1 and 2, 3 and 4, and 5 and 6, respectively.

4.1 Body Alone

4.1.1 *Cases of Khan and Chung*

Figures 5 through 8 provide the groove effects on body alone of Reference 3. For models 2 100 and 4 100, the increase is about +4%, as depicted in Figure 5. For the models 2200 and 4200, the changes are larger and amount to +9% to +14%, as given in Figure 6. For models 2400 and 4400, the changes are about +4%, as shown in Figure 7. Also, for models 2500 and 4500, the changes are only +5%, as given in Figure 8. The explanation made for the larger values for models 2200 and 4200 is that the nose-end section has a sudden step-down junction with the body, which must have caused further flow disturbance ahead of the grooves and larger lift increase. Therefore, this step-down effect was reflected by the factor F_2 in Equation (8).

4.1.2 *Cases of Brandon and von Wahlde*

Figures 9 through 14 provide the results for the body alone of Brandon and von Wahlde. Figures 9 through 11 provide the F_b factor at Mach = 5 for the three grooving types. The grooves increase the normal force by about +5% to +8%. The effect increases with the length of the grooves. Figures 12 through 14 depict the variation of the effect with Mach number for three different body-alone lengths. The groove effect decreases slightly with increasing Mach number and is about +7% for the three different body lengths.

4.1.3 *Cases of Sigal*

Figure 15 shows the correlation result for the wind tunnel test of Sigal.[5] The groove effect increased with the increased pitch of the grooves. The values increased from +8% to +12% approximately. One should note that increasing the groove pitch is limited to about $p = 0.25$ inch, beyond which, each groove tooth may act as a separate single cavity, with different flow phenomena than the present close-grooves study, as was emphasized in the introduction section.

4.2 Body With Fins

4.2.1 Cases of *Brandon and von Wahlde*

Reference 4 of Brandon and von Wahlde provides fewer results for a body with fins than for body alone. Most of the tests were performed at Mach = 5 and for the L/d = 25.6 configuration. It was noticed that the closeness of the end of the groove length to the beginning of the most forward point at the fin root has a relatively large effect on the amount of loss of the fin normal force. When the second grooved section of the body (nearest the fins) was replaced by a smooth body section, the grooves effect on the normal force of the total vehicle was much reduced from 3.8% to about 1 .0%, as can be seen in Figure 16 for the G/S case. For the fully grooved body, the total vehicle lift loss was about -4%.

4.2.2 *Cases of Sigal*

The results for the data of Sigal[5] for a finned body at Mach 2.4 are shown in Figure 17. What was surprising from this test is the relatively large difference in results for the fins in the + and x roll position. In the + fin formation, only two fins are producing lift and are affected; thus, the fin lift loss contribution to the total vehicle lift is small. This small decrease in fin losses cannot outweigh the positive increase in lift attained by the body alone, thus resulting in a net increase of the lift of the total body of about +3% to +4%. For fins in the x formation, the four

fins are producing lift and are all affected by the grooves. Thus, the decrease in fin lift counters the increase attributable to the body alone, with a net decrease of about -1% to -2% for the total vehicle. This example is a good application of the present analysis of the body-alone and fin-in-the-presence-of-a-body models. Through the present model, an explanation for the observed results was possible.

4.3 Body With Flare

4.3.1 *Cases of Sigal*

A case of body with a stabilizing conical flare was tested and presented in Reference 5. The established correlation results for the few cases tested at Mach 2.4 are shown in Figure 18. From the given data, the grooves are shown to cause an increase in the total vehicle lift, as was the case for body alone, but the fin cases suffer a decrease in lift production. Unfortunately, there are no additional data cases to ascertain the accuracy of the predictions for other flare angles or at other Mach numbers. The case of the knurled surface seems either to have been mis-measured or to have provided a much smaller effect on the flare. In the prior cases for knurled surfaces for both the body alone and body with fins (Figures 15 and 17, respectively), the knurled surface (as a smaller surface roughness) provided more consistent values with regard to the magnitude of the increase in normal force. For the present case of 7.1 ° half cone flare angle at Mach 2.4, the normal force increase varied from +6% to +14% as the grooving effect increased because of the increased groove pitch.

4.4 Validation Cases of Fellows-Carberry and Hendry

The test data provided by Fellows and Carberry[6] and reported by Hendry[7] were not used in constructing the correlation but were left for an independent application after the completion of the correlation. This is attributable to an apparent inconsistency in the data that may be considered measurement errors, especially given the small differences, as explained earlier in the error estimation section.

The code of Reference 12 was used to compute the CN_α (which is depicted in Figure 4) for smooth body alone and body with fins for the six-firmed configuration of References 6 and 7. The scatter in the test data is shown in Figure 19 which reflects the variation of F_{bf} with both Mach and Reynolds numbers. This comparison was made for the configuration having separate front and rear grooved sections. The other two groove configuration types showed more inconsistent results. The present correlation for a body with fins provided what is believed to be

well-represented effects of the total vehicle lift loss of about -2% to -5% over the speed regime of Mach 5 to 2 and varying Reynolds number between 2.5×10^6 and 17.8×10^6 per foot (see Table 5 for cases 48 through 5 1). The present analysis predicted the correct sign and provided good estimates for the change in the lift force because of grooves.

4.5 Comnutational Fluid Dvnamics (CFD) Calculations of Forkois[13]

CFD computations were not expected to have been made for grooved bodies. The actual grooves have sharp contour lines and may require a large number of grid points near each corner of each groove. In addition, the effect was thought not to be large enough to invite a large CFD effort. However, one set of unpublished CFD calculations was reported in Reference 13. Computations were made to investigate the suspected groove effect on lift and the stability of a firmed projectile. A parabolized Navier-Stokes (PNS) code was used. Two other minor fin shape variations were considered and computed. Only three calculations for body with the three fin shapes were computed at Mach 5.44. For each case, computations were made for smooth and grooved body. No body-alone computations were made. Computations were made for four fins in the + formation at 1 ° angle of attack. The Reynolds number was 3.2×10^6, based on the total body length. The body diameter is 0.284 inch (7.22 mm) and the configuration is shown in Figure 20. The actual physical grooves are 0.02 inch deep and have a pitch of 0.083 inch (i.e., 12.0 grooves per inch). The grooves were geometrically simplified and modeled for computation as a sinusoidal wave depth of only 0.004 inch (i.e., one fifth of the actual depth) to allow continuous contoured body surface coordinates and grids to be used. The configuration total L/d ratio is 24.5 and the grooved body length is 16.3 calibers. There are 52 grooves modeled along that length. No grid-refinement studies were performed, and the groove effects on the total normal force were, not surprisingly, almost identical for the slightly different fins.

Because of the mentioned geometrical simplifications of the grooves, CFD computations were not relied on for either establishing the correlations or validating their outcome. One might compare the results to assess whether CFD predictions will exceed or underestimate the value. For the projectile considered, CFD predicts -6.6% reduction in the total normal force. This value appears to be large since the normal force for this configuration is dominated by the long body and not by the four small fins. This means that the lift increase attributable to the long body may not be offset by the decrease attributable to the small fins; thus, it should result in a net increase rather than a net decrease in the total normal force, relative to the smooth-body case. The present correlation was applied, and the NSWC-AP95 code[12] was used to estimate the smooth-body values of the CN_α of 4.975 for the total vehicle; the body alone contributed 4.195 or 84.3%

of the total. The F_b, F_f, and F_{bf} for fm configuration No. 2 were computed as t-O.03 16, -0.0175, and +0.0092, respectively. This indicates a net total increase in lift of +0.92%, rather than the predicted -6.6% loss. The results are shown in Figure 21. It is believed that reducing the groove depth for CFD and modeling the grooves as a continuous smooth sinusoidal wave have significantly reduced the body-alone contribution, thus affecting the results. In addition, it is not known if a finer grid, especially near the surface, would have changed the computational outcome.

5. **PREDICTIVE DESIGN EXAMPLE**

A design example for two different KE projectile configurations is given. In the first one, the total normal force will increase, while in the second, it will decrease. It would have been surprising for a wind tunnel test of both models (under the same flow conditions) to provide such a contradictory outcome. The present analysis and correlations provide the reason and the magnitude of change for both cases. This application is an illustration of the use of the present work.

Both configurations have a l-inch diameter and 3.5-caliber-long sharp conical nose. A hypothetical wind tunnel test at Mach = 5, Reynolds number of 5.0×10^6 per foot, at zero fin roll angle is simulated. The first configuration has an L/d ratio of 28.0 and the second model has an L/d of 13.0. Both have a groove pitch of 0.125 inch (eight grooves per inch).   The first projectile has a grooved length of 20.5 calibers, while the second has grooved length of only 5.5 calibers. Both configurations have trapezoidal fin planforms. The first model has four small fins, with a root chord of 3.0 calibers' length, while the second has six fins with a 4.0-caliber root chord. The fin taper ratios are 0.08 and 0.70, respectively. The fin aspect ratio values are 0.36 and 0.42, respectively. The two configurations are shown in Figure 22.

The smooth-body normal force slope coefficients were computed using the fast aerodynamics prediction code of Reference 12. The first model has body alone and total body CN_α values of 4.29 and 6.42, respectively. The second model similarly has CN_α values of 3.83 and 11.65, respectively. The first model has total normal force to body-alone value ratio of 1.49, while the second model's ratio is 3.04. The body-alone normal force factor, F_b, is computed to be +0.074 and +0.042 for the first and second models, respectively. The fin-correction factor, F_f, is -0.013 and -0.049 for the first and second models, respectively. The total normal force change factor, F_{bf}, is +0.036 and -0.035 for the first and second models, respectively. Therefore, a wind tunnel test would have shown a change in lift of +3.6% for the first model and a change of -3.5% for the second model, over the corresponding smooth-body values. These wind turmel test results would

have been misinterpreted as "inconsistent" or "contradictory." The present work not only explains these results but also quantifies the effect.

6. **CONCLUSIONS AND SUMMARY**

The results of the present correlations and the experimental data upon which they were based are shown in Figure 23 for 44 cases, reflecting good agreement.

Based on the experimental data analyzed and the empirical correlations that were constructed and reflect them, the following conclusions are drawn for supersonic speeds and small angles of attack faced by most anti-armor projectiles:

1. An empirical model for KE projectiles based on experimental data for different shapes, fins, and speeds was developed and yielded fast, accurate predictions for the incremental lift attributable to surface grooves.

2. For body alone, body grooves always result in increasing the body normal force over the corresponding smooth-body value. The largest increase observed was about +15%.

3. Body surface grooves always decrease the fin-in-the-presence-of-a-body normal force from the corresponding smooth-body value.

4. A body-fin combination may have higher or lower total vehicle normal force relative to the smooth-body value, depending on the relative length of the body, the grooved section length, and the size and number of fins. The largest lift loss observed in this study was about -5%.

5. For body with flare, the grooves tend to increase the normal force, as if the flare were just an extension of the body alone. The largest value observed was about +15% over the smooth-body value.

6. The location of the grooves on body alone does not seem to be an influential factor. For body alone, a short grooved section of the body positioned after the nose caused almost the same lift increase percentage as if the whole body were grooved.

7. The groove effect on normal force decreases with increasing flow Mach number. This is for both body alone, fin in the presence of a body, and thus for the total vehicle.

8. The fin roll orientation angle angle has a surprisingly relatively large influence on the fin lift loss for cruciform fins. This effect is predicted to be less for six-fin configurations (or generally, fin numbers larger than four).

9. CFD computations for a shallow, wavy groove profile (replacing the sharp and deep actual grooves) tend to overpredict the effect of grooves on the finned body total normal force. For the case studied, CFD predicts -6.6% normal force decrease, while the present correlations provide +0.9% increase for the case of four small fins, long body, and high Mach number.

In summary, the present work provides a fast, simple method to estimate the incremental change in the normal force slope coefficient (and thus the normal force coefficient) for body alone and body with fins, which is caused by standard (i.e., typical) grooves on the projectile body. The method is based on empirical correlations that are based on experimental data. Most of the projectile, fin, and flow parameters are included. A correlation for flared bodies was also derived, based on limited data, and should be further validated or modified when future tests and more geometry variation results become available. The established correlations provide the direct incremental change in the normal force slope coefficient as a fraction of the corresponding smooth-body value which is more easily available from fast aerodynamic design codes. The present correlations can also be included in these codes, thus providing a fast estimate for the groove effects.

For future studies, a similar fast method may be established to determine the corresponding change in location of the center of pressure (caused by grooves) for body alone and body with fins or flares.

Table 1. Body Alone: Case Designation and Test Conditions

Case No.	Ref.	Test Model or Run No.	Total Length, I (caliber)	l_{g1} (cal.)	T_1 Type	l_{g2} (cal.)	T_2 Type	Mach No.	Re per ft x 10⁻
1		2100	21.86						
2		2200	21.80	3.9		—	—		
3		2400	20.94						
4	Khan & Chung	2500	21.80		I' (32 pi)			4.0	1.4
5		4100	21.86						
6		4200	21.80	18.6		—	—		
7		4400	20.94						
8		4500	21.80						
9		3					T (32 pi)	3.5	4.0
10		21	20.59	6.4		4.0	S		
11		24					T (32 pi)	5.0	5.6
12		26					G (8 pi)		
13		4					T (32pi)	3.5	4.0
14		14					T (32 pi)	4.0	4.8
15		33	25.59	9.6		6.0	S		
16	Brandon & von Wahlde	39					T (32 pi)	5.0	5.6
17		56			? (8 pi)		G (8 pi)		
18		59					S		
19		61	30.58	2.4		8.0	T (32 pi)	5.0	5.6
20		62					G (8 pi)		
21		11					T (32 pi)	3.5	4.0
22		19					T (32pi)	4.0	4.8
23		72	35.59	5.4		10.0	S		
24		73					T (32 pi)	5.0	5.6
25		74					G (8 pi)		
26		—			K	—	—		
27	Sigal	—	13.50	8.0	T (25.4 pi)	—	—	2.4	25.9
28		—			G_1 (12.7 pi)	—	—		
29		—			G_2 (6.35 pi)	—	—		

S = Smooth Surface   G = Grooved   pi = (grooves) per inch
T = Threaded   K = Knurled   cal. = caliber

Table 2. Body Alone: Comparison With Data

Case No.	CN,, Wind Tunnel			$(\Delta CN_{\alpha g}/CN_{\alpha s})$	
	Grooved (1)	Smooth (2)	A $CN_{\alpha g}$= (1) - (2)	Wind Tunnel	Present Predictions
1	3.80'	3.70	+0.10	+0.027	+0.026
2	4.35	3.90	+0.45	+0.102	+0.088
3	4.05'	3.90	+0.15	+0.038	+0.032
4	3.90	3.75	+0.15	+0.040	+0.041
5	3.85	3.70	+0.15	+0.041	+0.043
6	4.45	3.90	+0.55	+0.141	+0.147
7	4.10	3.90	+0.20	+0.051	+0.053
8	4.00	3.75	+0.25	+0.067	+0.068
9	3.39‡	3.19	+0.20	+0.063	+0.072
10	3.29		+0.17	+0.054	+0.054
11	3.31	3.12	+0.19	+0.061	+0.063
12	3.35		+0.22	+0.074	+0.074
13	3.81	3.54	+0.27	+0.076	+0.078
14	3.74‡	3.48	+0.26	+0.075	+0.074
15	3.63		+0.19	+0.060	+0.059
16	3.66	3.42	+0.24	+0.070	+0.068
17	3.69		+0.27	+0.079	+0.077
18	3.87		+0.23	+0.063	+0.063
19	3.91	3.64	+0.27	+0.074	+0.073
20	3.93‡		+0.29	+0.080	+0.082
21	4.45	4.12	+0.33	+0.080	+0.086
22	4.42	4.10	+0.32	+0.078	+0.082
23	4.33		+0.26	+0.065	+0.066
24	4.38	4.07	+0.31	+0.076	+0.076
25	4.40		+0.33	+0.081	+0.084
26	2.94		+0.22	+0.080	+0.082
27	2.97†	2.72	+0.25	+0.092	+0.089
28	2.99		+0.27	+0.099	+0.110
29	3.03		+0.31	+0.114	+0.119

† Corrected value ‡ Adjusted value due to asymmetry

Table 3. Body With Flare: Case Designation and Test Conditions

Case No.	Ref.	Total Length, L (caliber)	l_{g1} (cal.)	T_1 Type	l_{g2} (cal.)	T_2 Type	Axial Length (caliber) and Flare Half-Angel (degree)	Mach No.	Re per ft $\times 10^{-6}$
30	Sigal	13.8	8.0	K	—	—	1.17 and 7.12.'	2.4	25.9
31				T (24.5 pi)					
32				G_1 (12.7 pi)					
33				G_2 (6.35 pi)					

K = Knurled   T = Threaded   G = Grooved   pi = (grooves) per inch   cal. = caliber

Table 4. Body With Flare: Comparison With Data

Case No.	CN_α, Wind Tunnel			$(\Delta CN_{\alpha g}/CN_{\alpha s})$	
	Grooved (1)	Smooth (2)	$\Delta CN_{\alpha g}$ = (1)-(2)	Wind Tunnel	Resent Predictions
30	4.30	4.20	+0.10	+0.024	to.075
31	4.62		+0.40	+0.100	+0.085
32	4.73		+0.53	+0.126	+0.110
33	4.81		i-0.61	+0.145	+0.144

21

Table 5. Body With Fins: Case Designation and Test Conditions

Case No.	Ref.	Total Length, L (cal.)	Length and Type of Grooves				Number, Type, Orientation of Fins	Mach No.	Re per ft × 10⁻⁶
			l_{g1} (cal.)	T₁ Type	l_{g2} (cal.)	T₂ Type			
34	Brandon & von Wahlde	25.59	9.4	G (8 pi)	6.0	S	Six Fins, Clipped delta,	5.0	5.6
35						T (32 pi)			
36						G (8 pi)			
37	Sigal	13.5	8.0	K	—	—	Four Fins, Clipped delta,	2.4	25.9
38				T (25.4 pi)	—	—			
39				G1 (12.7 pi)	—	—			
40				G2 (6.35 pi)	—	—			
41				K	—	—	Four Fins, Clipped delta,		
42				T (25.4 pi)	—	—			
43				G1 (12.7 pi)	—	—			
44				G2 (6.35 pi)	—	—			
45	Forkois (CFD)	24.5	16.5	G (12.0 pi)	—	—	Fin 1 / Four Fins,	5.44	5.5
46							Fin 2		
47							Fin 3		
48	Fellows & Carberry (Application)	16.1	1.5?	G (8.0 pi)	153	G (8 pi)	Six Fins, Clipped delta,	4.9	15.5
49								4.0	17.8
50								3.0	2.5
51								2.0	3.6

S = Smooth Surface   G = Grooved   pi = (grooves) per inch
T-Threaded   K = Knurled   cal. = caliber

Table 6. Body With Fins: Comparison With Data

Case NO.	CN_{α}, Wind Tunnel			$(\Delta CN_{\alpha g}/CN_{\alpha g})$	
	Grooved (1)	Smooth (2)	$\Delta CN_{\alpha g}$ = (1) − (2)	Wind Tunnel	Present Predictions
34	12.23		-0.11	-0.009	-0.013
35	11.92‡	12.34	-0.42	-0.034	-0.039
36	11.86		-0.48	-0.039	-0.045
37	5.31†		-0.04	-0.007	-0.009
38	5.24	5.35	-0.11	-0.020	-0.010
39	5.25		-0.10	-0.020	-0.017
40	5.24		-0.11	-0.020	-0.020
41	5.34†		+0.17	+0.033	+0.030
42	5.36	5.17	+0.19	+0.037	+0.033
43	5.37		+0.20	+0.039	+0.036
44	5.40		+0.23	+0.044	+0.043
45	5.05	5.41	-0.36	-0.067	+0.015
46	5.78	6.18	-0.40	-0.064	+0.009
47	5.50	5.90	-0.40	-0.068	+0.012
48	9.00	9.20	-0.20	-0.022	-0.032
49	9.20	10.05	-0.85	-0.085	-0.052
50	11.10	11.75	-0.65	-0.055	-0.023
51	13.50	13.70	-0.20	-0.015	-0.041

† Corrected Value   ‡ Adjusted value due to asymmetry
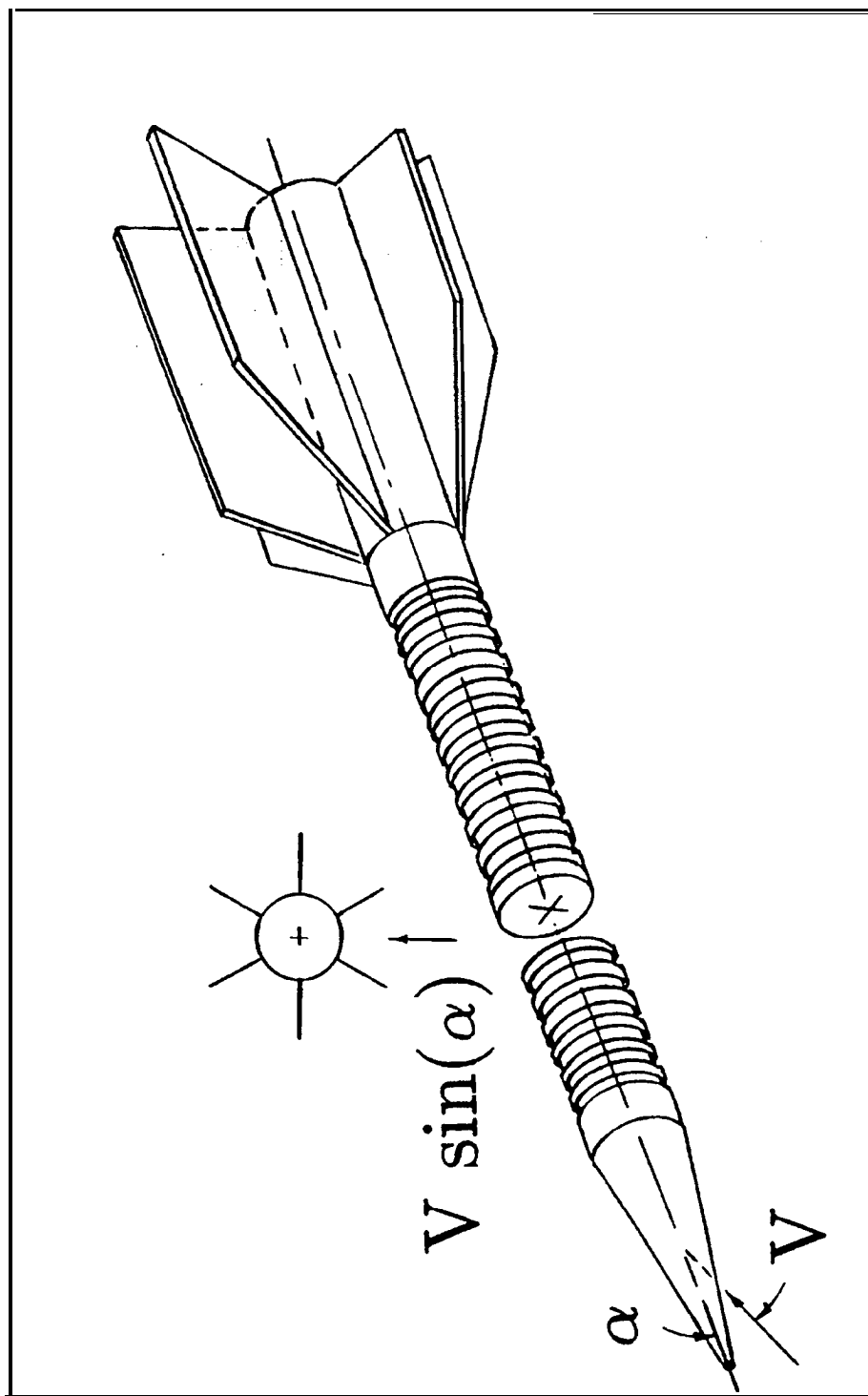
Figure 1. Grooves of the Typical KE Projectile.

$V \sin(\alpha)$

α

V
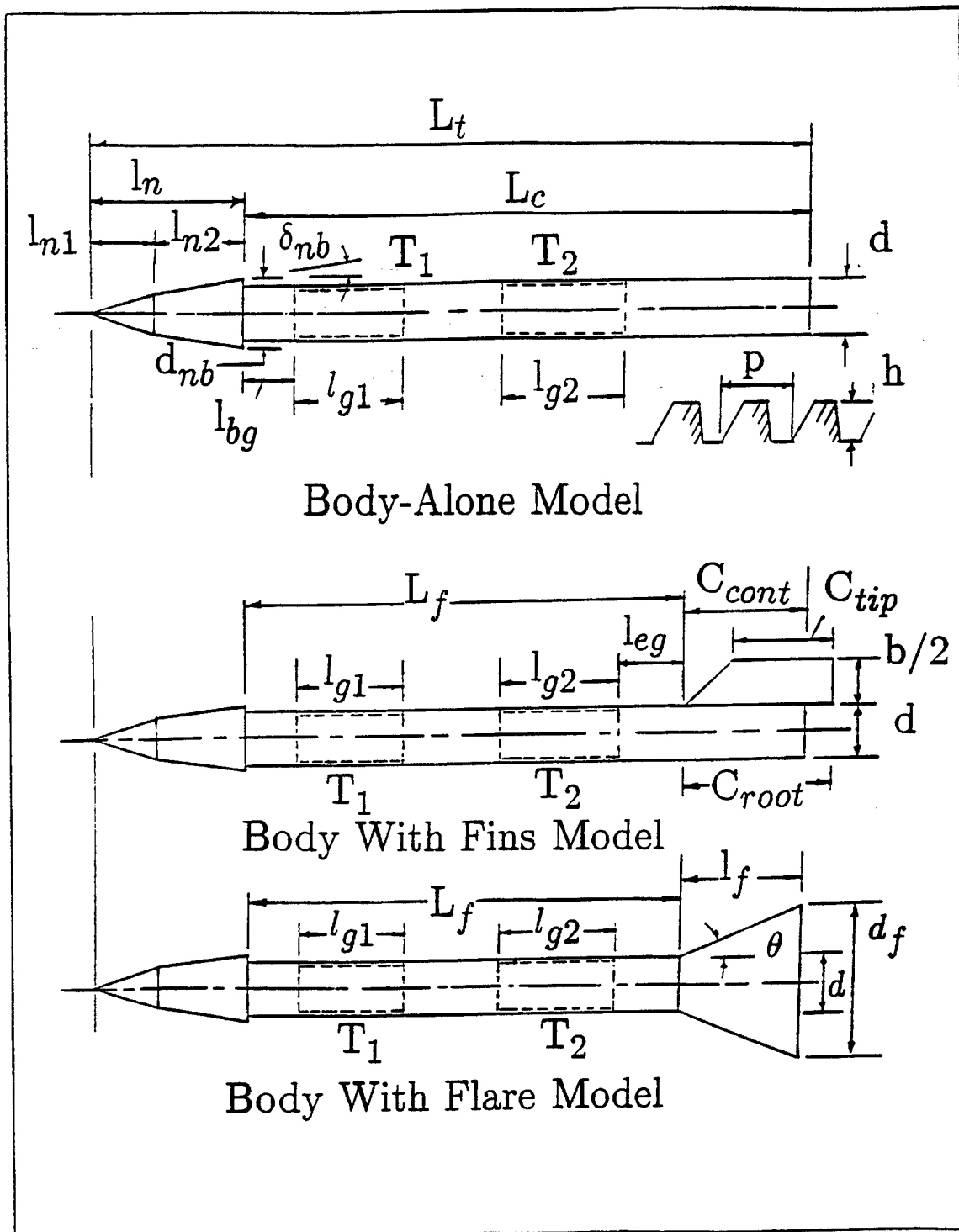
Figure 2. Nomenclature for the Present Correlations.

FIN — AFT BODY — FORE BODY — NOSE

L_AFT

.938 DIA.

4.170

AFT BODY - SMOOTH

L_FORE

1.000 DIA.

FOREBODY - SMOOTH

L_AFT

.938 DIA.- 30 THREADS/CALIBER

4.170

AFT BODY - THREADED

L_FORE

1.000 DIA.

DETAIL A   DETAIL B

FOREBODY - GROOVED

L_AFT

4.170

AFT BODY - GROOVED
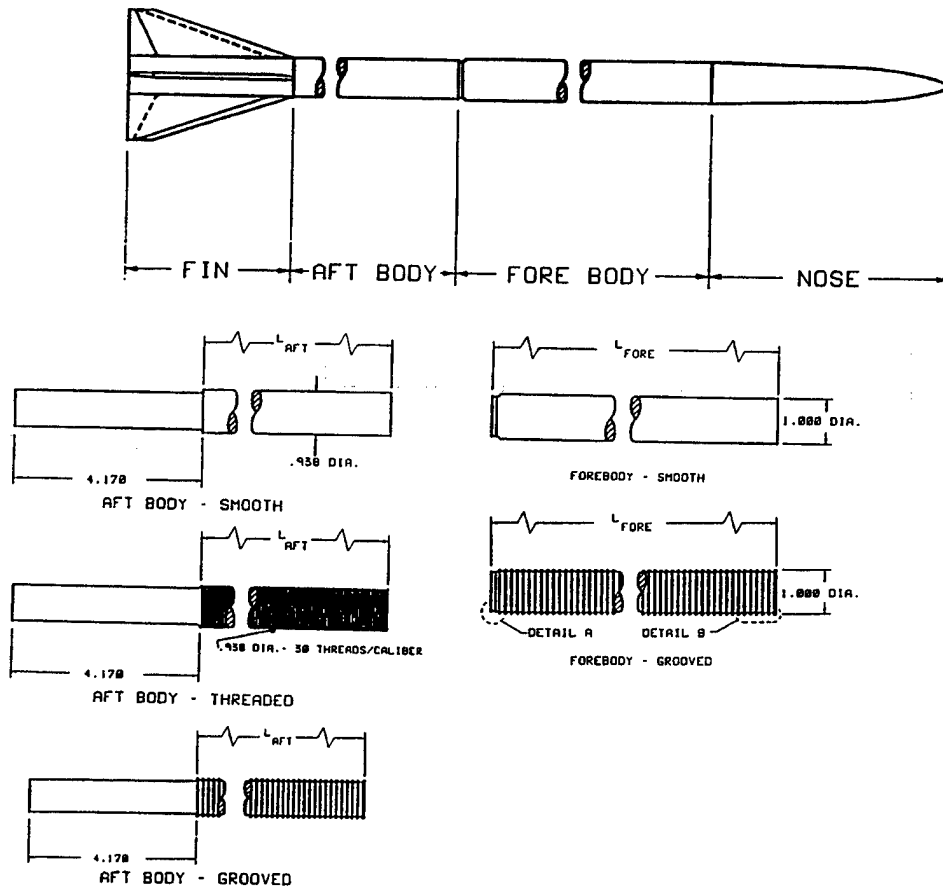
Figure 3. Test Model and Grooves of Brandon and von Wahlde.[4]

708·0

135·6   130·3   4·1   MRP   268·7   124·5   24·5

44·0   106·6

352·5   42·6

CONFIG 05

107·3   4·1   67·18   4·1   126·15   4·1   67·18   4·1

CONFIG 12

DRAWN

⅓ MODEL SCALE

424·9

174·48   4·1   134·35   4·1   73·18

DIMENSIONS IN MM.

CONFIG 13

390·21

CONFIG 14

DETAILS OF VARIOUS LENGTHS OF BUTTRESS THREAD
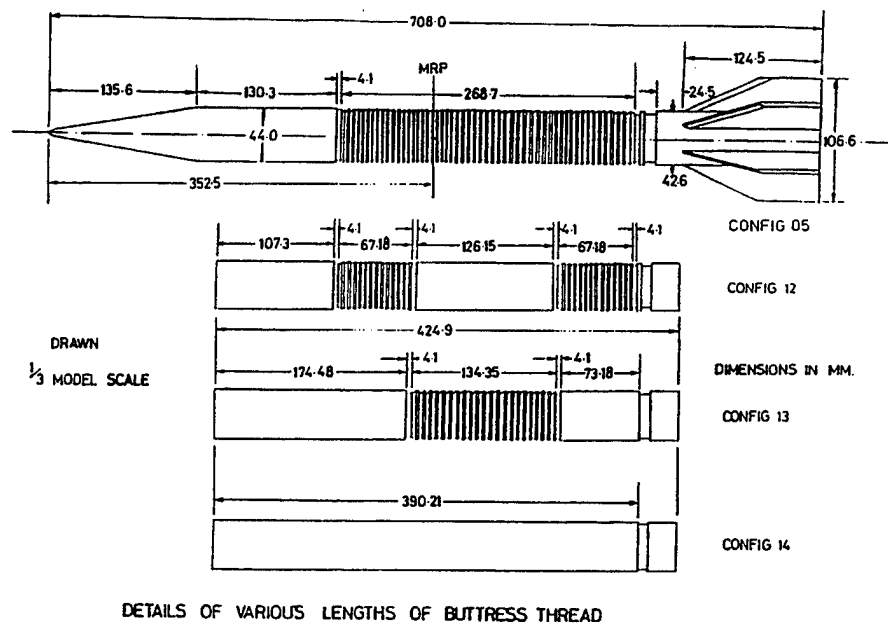
Figure 4. Test Model and Grooves of Fellows and Carberry.[6]

25
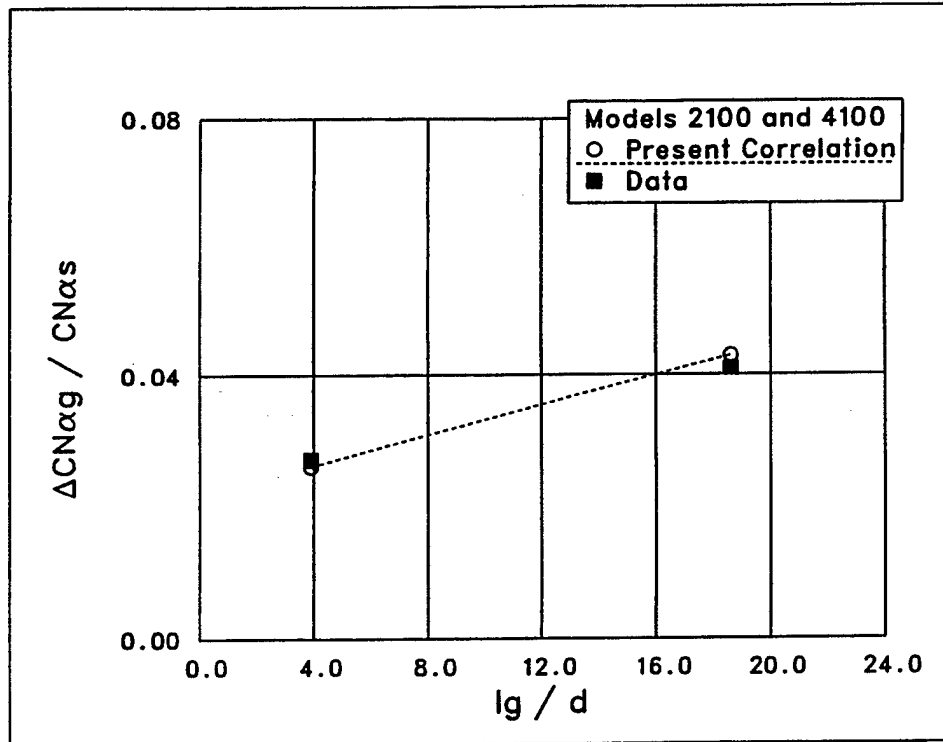
Figure 5. Results for Body Alone[3] (M = 4, Models 2100 and 4100).
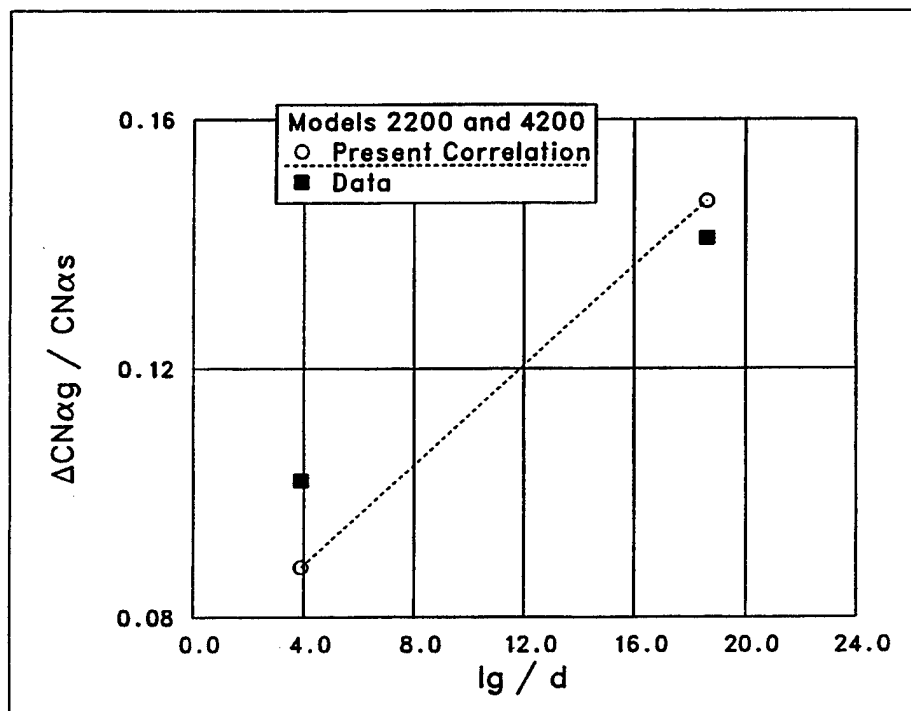
Figure 6. Results for Body Alone[3] (M = 4, Models 2200 and 4200).
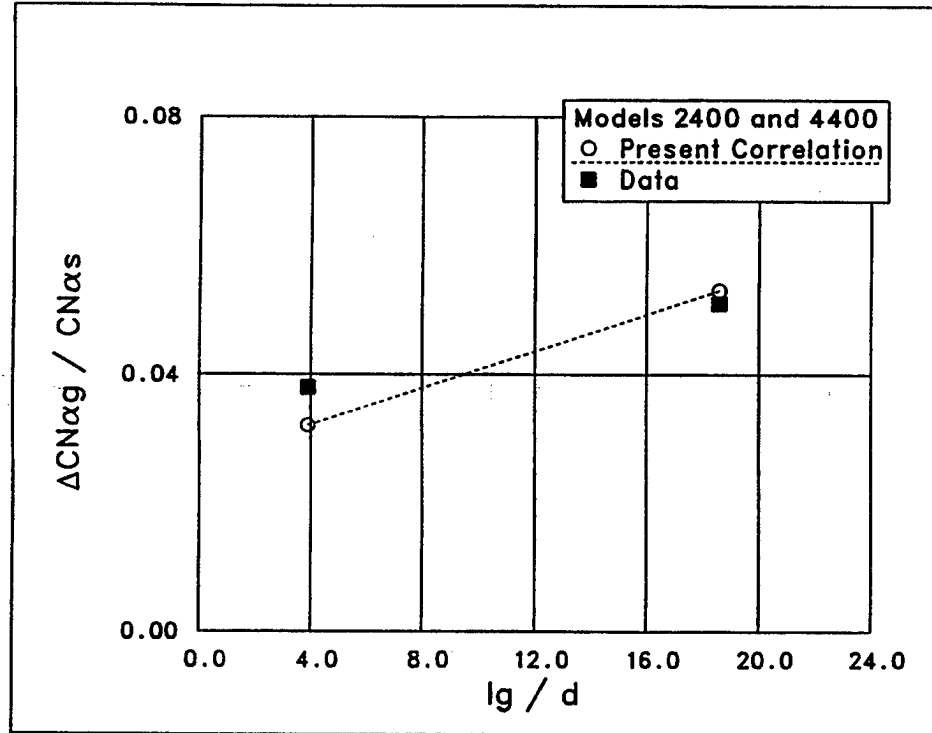
Figure 7. Results for Body Alone[3] (M = 4, Models 2400 and 4400).
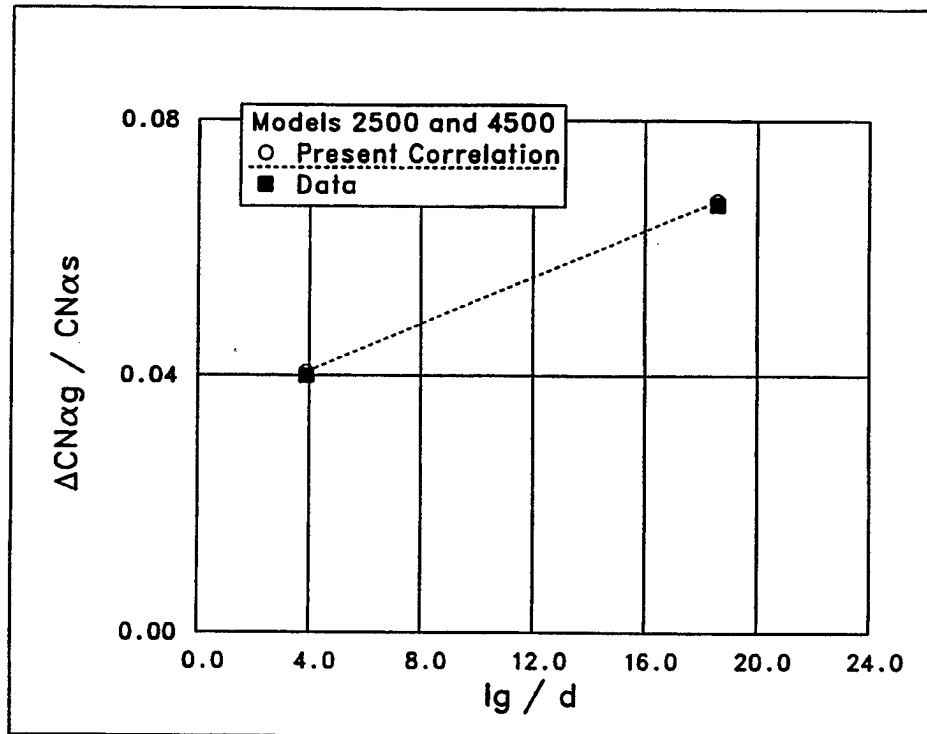
Figure 8. Results for Body Alone[3] (M = 4, Models 2500 and 4500).
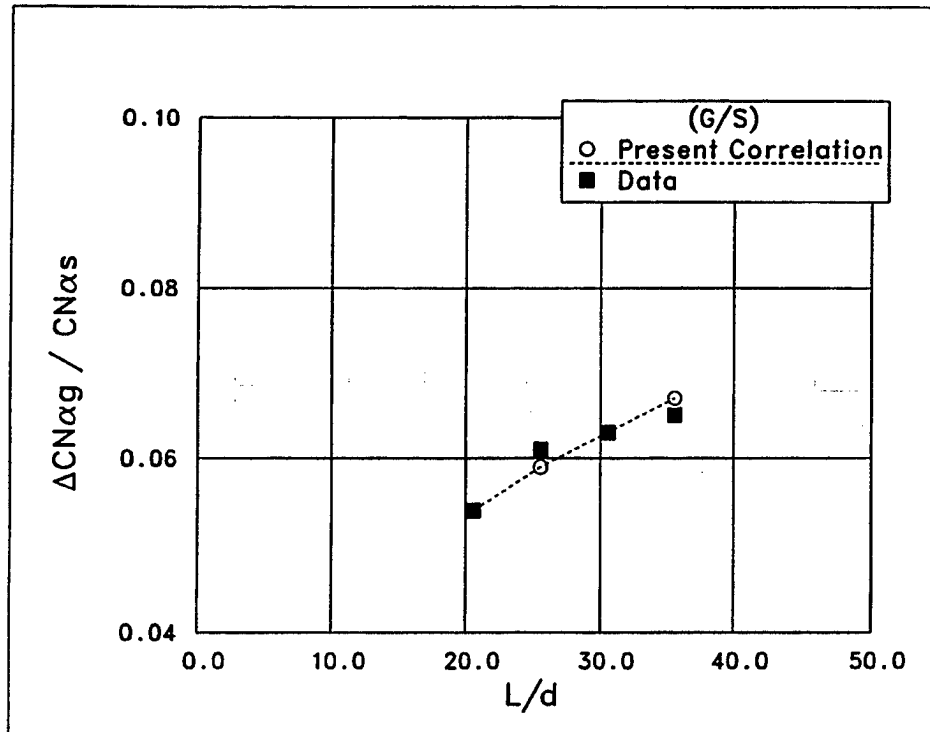
Figure 9. Results for Body Alone[4] (M = 5, G/S grooves).
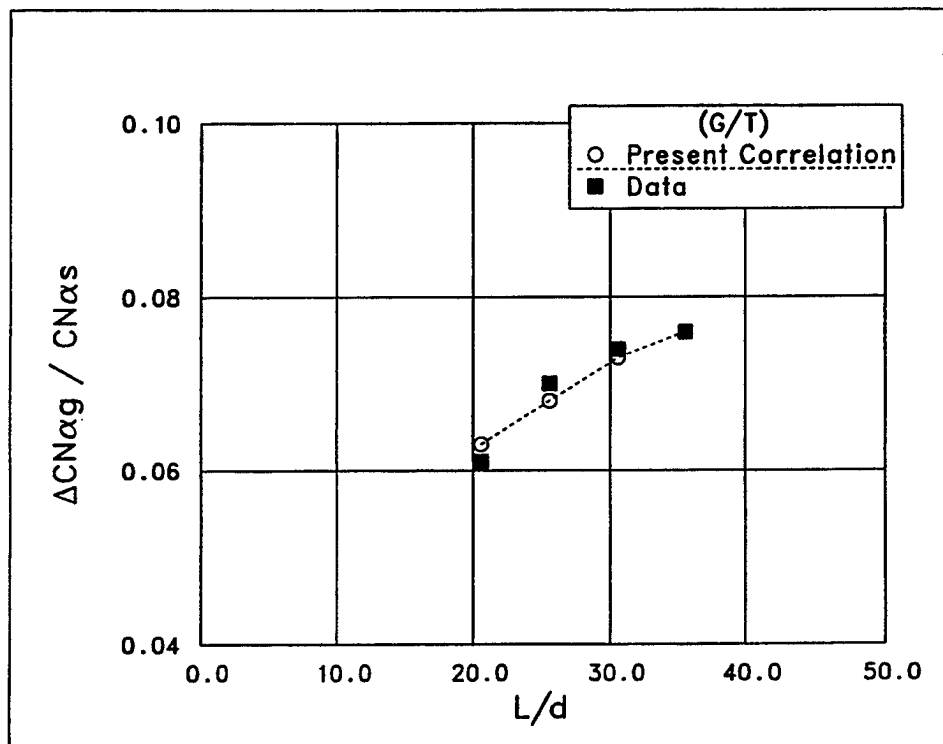
Figure 10. Results for Body Alone[4] (M = 5, G/T grooves).

28
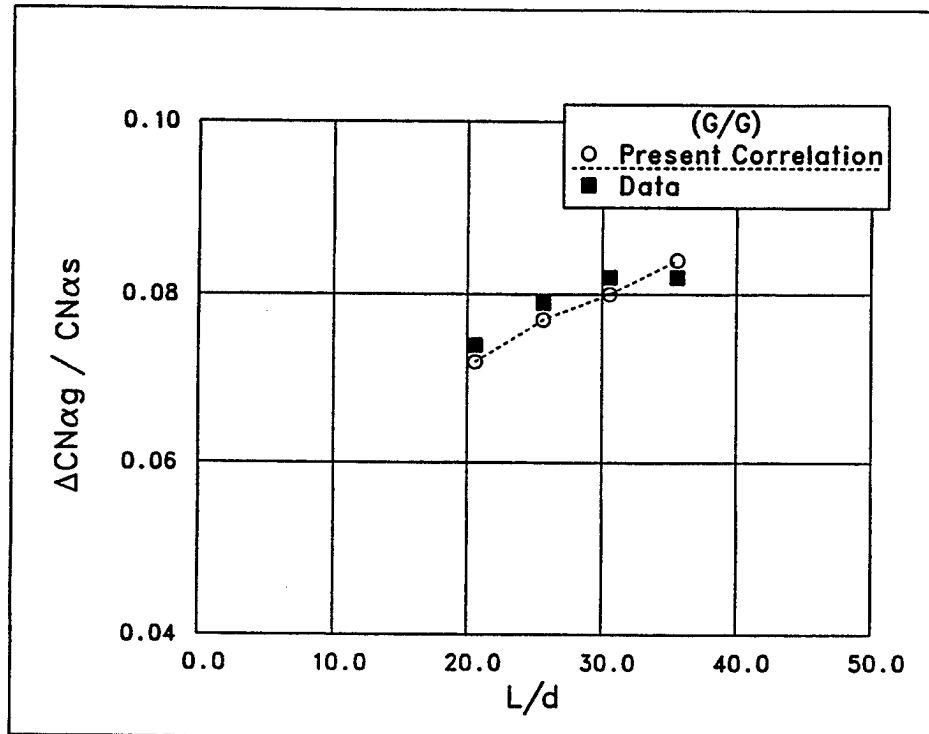
Figure 11. Results for Body Alone[4] (M = 5, G/G grooves).
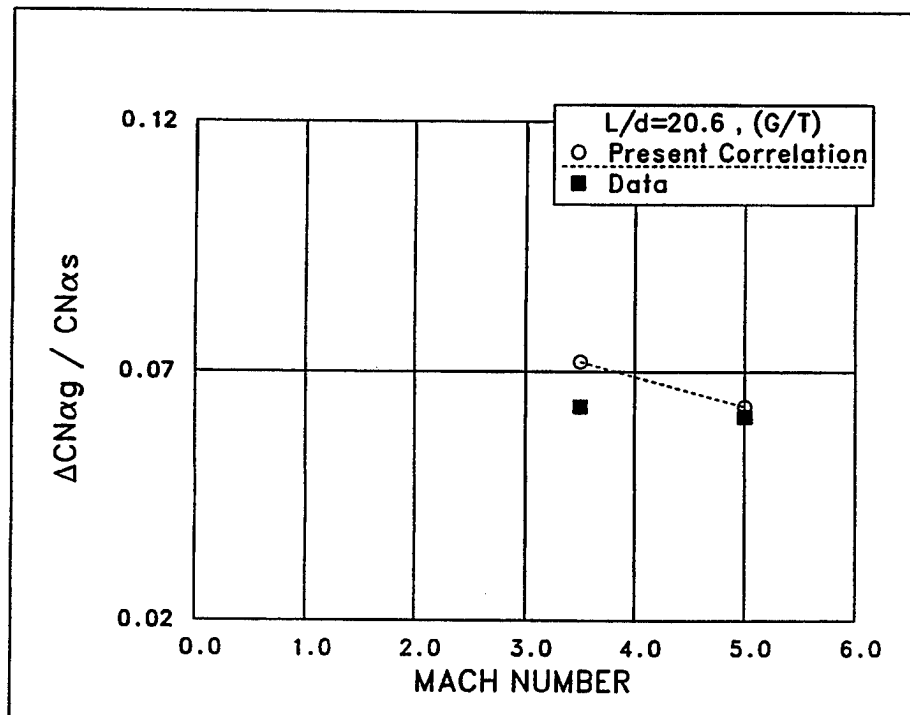
Figure 12. Results for Body Alone[4] (L/d = 20.6, G/T grooves).
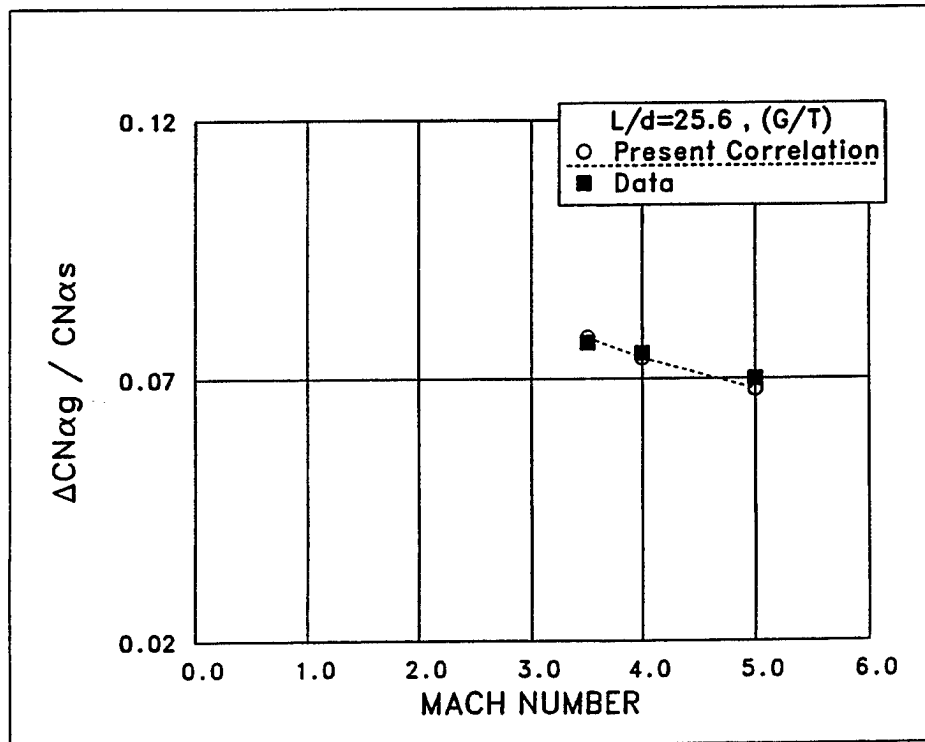
Figure 13. Results for Body Alone[4] (L/d = 25.6, G/T grooves).
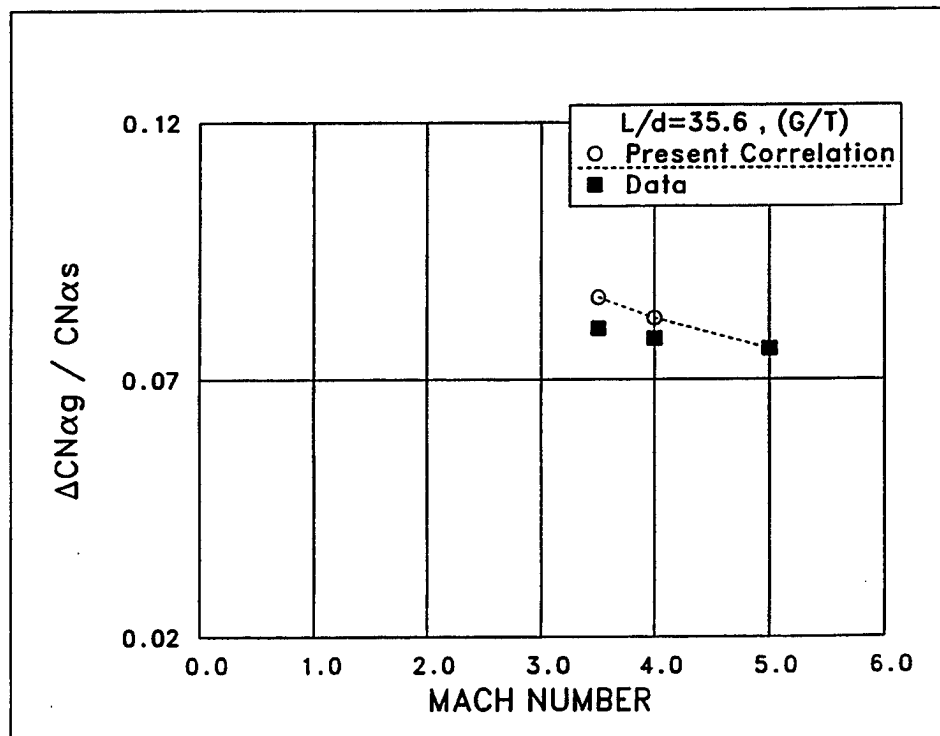
Figure 14. Results for Body Alone[4] (L/d = 35.6, G/G grooves).
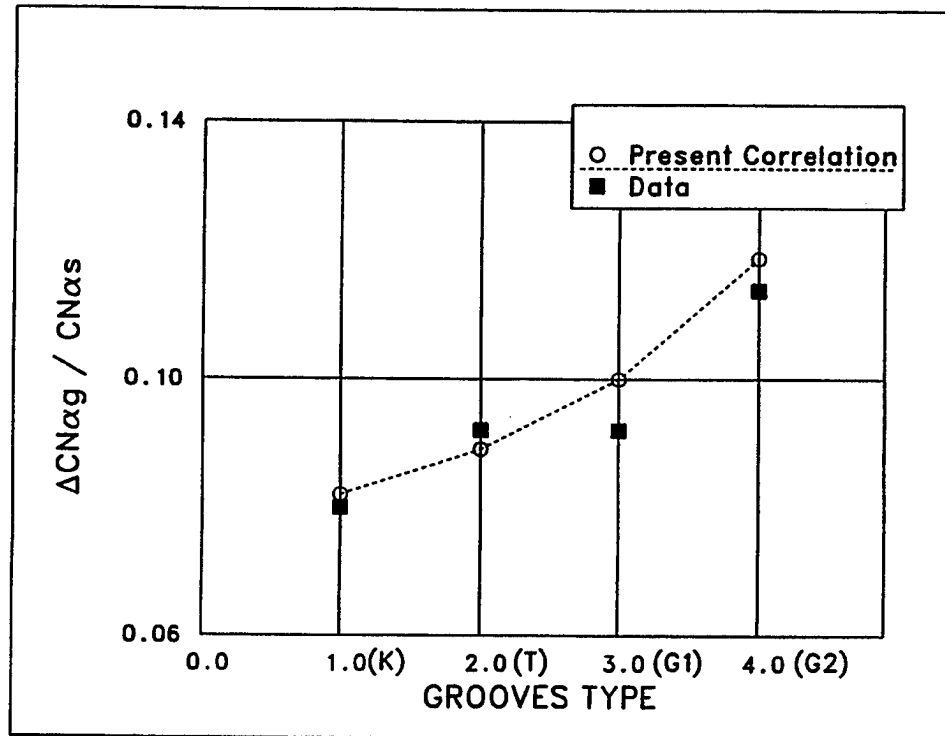
Figure 15. Results for Body Alone[5] (M = 2.4).
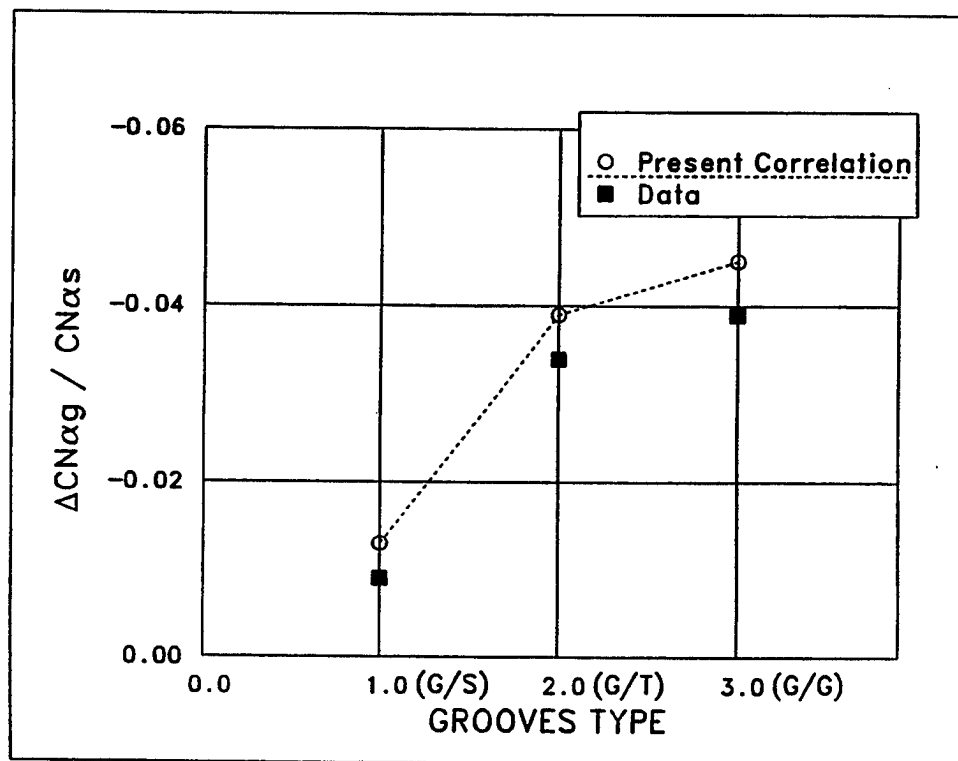
Figure 16. Results for Body With Fins[4] (M = 5, L/d = 25.6, six fins).
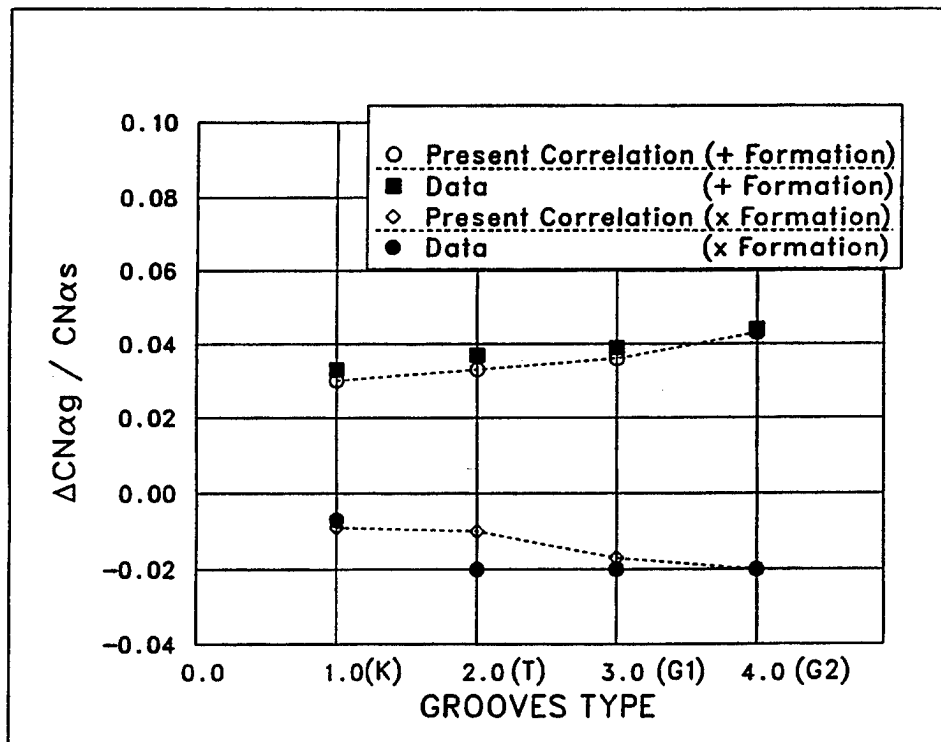
Figure 17. Results for Body With Fins[5] (M = 2.4, four fins).
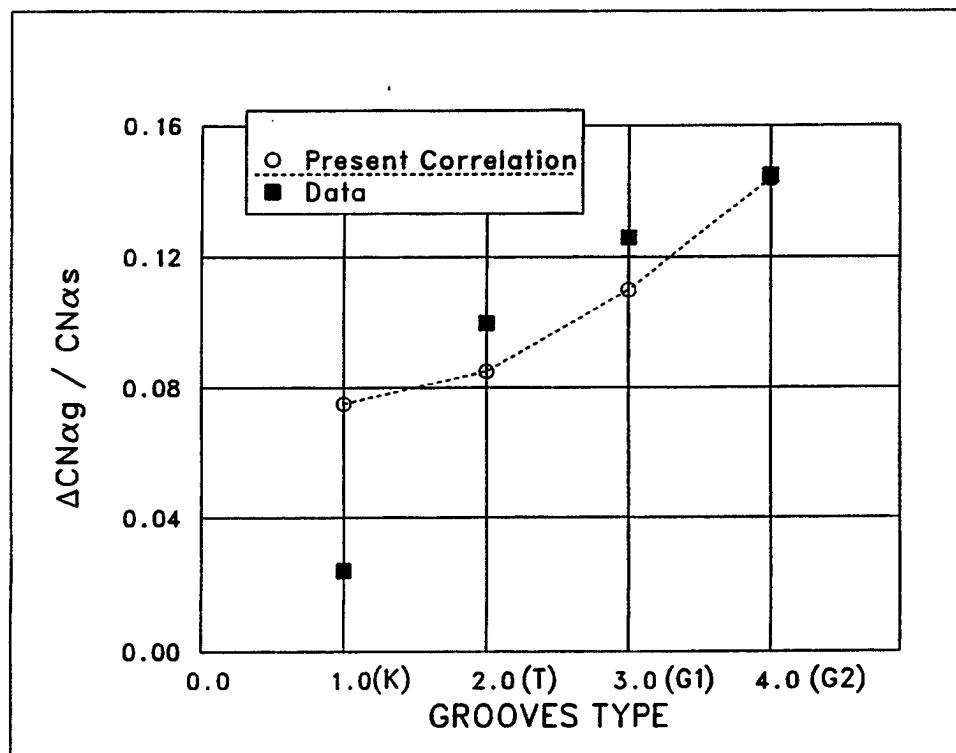
Figure 18. Results for Body With Flare[5] (M = 2.4).

32
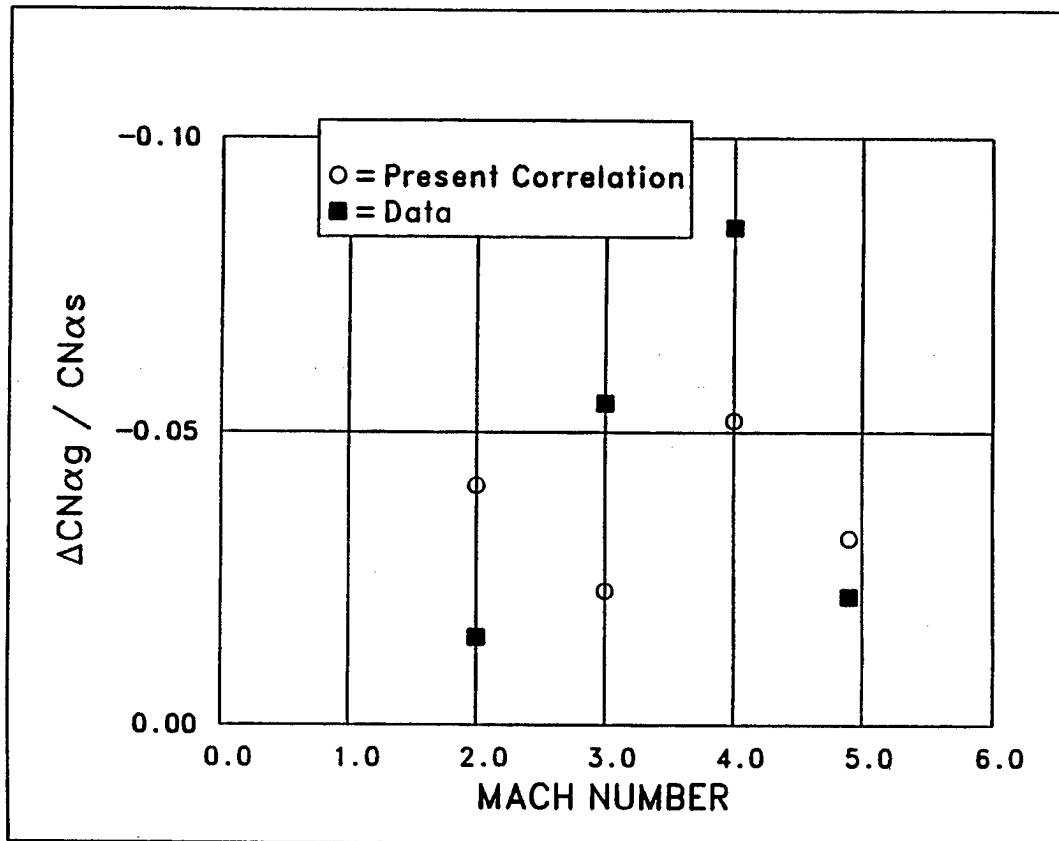
Figure 19. Results for Body With Fins[6] (varying Reynolds number, six fins).
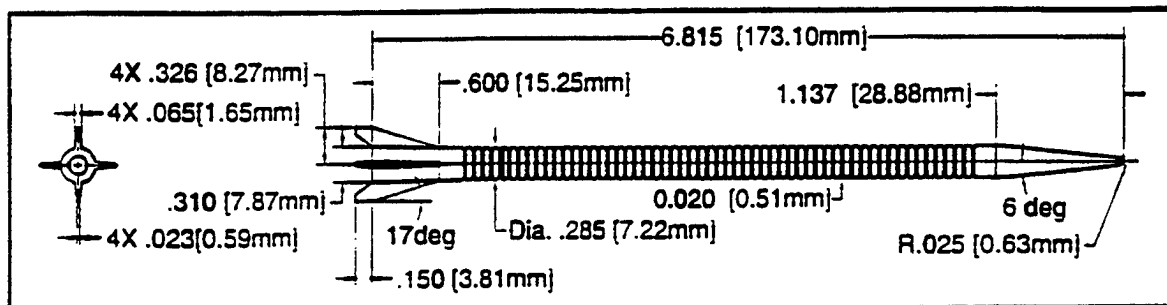
Figure 20. Projectile Configuration[13].
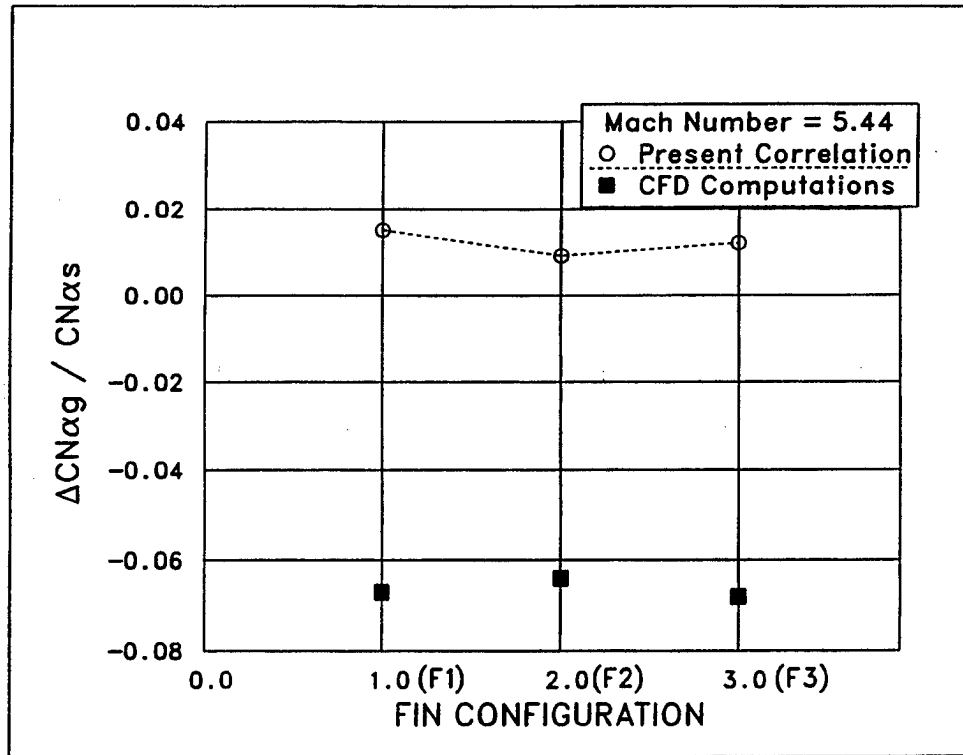
Figure 21. Results for Body With Fins[13] (CFD, M = 5.44, four fins).
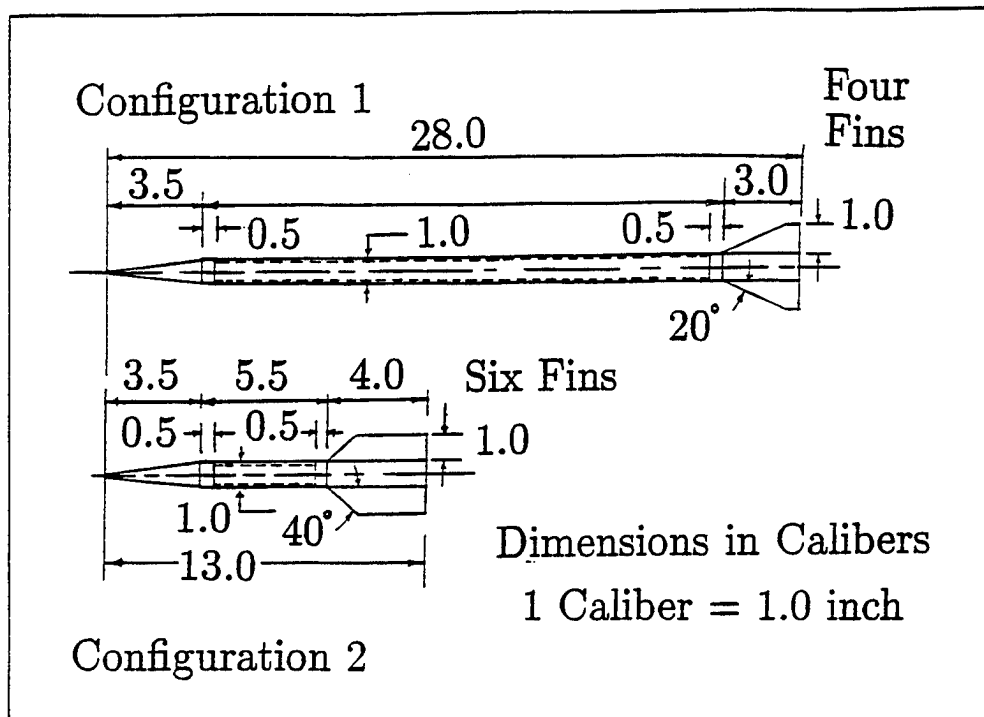
Figure 22. The Two Projectile Configurations of the Predictive Example.
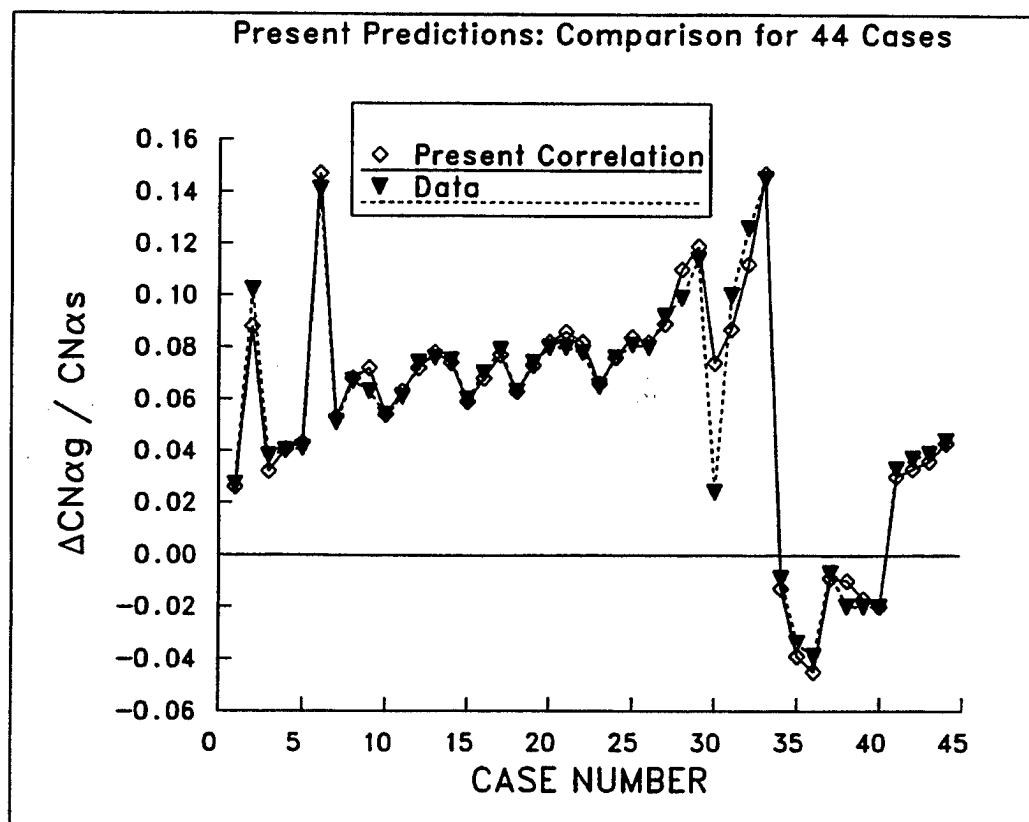
Figure 23. Overall Prediction Comparison With Data.

INTENTIONALLY LEFT BLANK

REFERENCES

1. Mikhail, A.G. "Drag Correlation and Prediction of Surface Groove Drag for Kinetic Energy Projectiles," AIAA Journal of Spacecraft and Rockets, Vol. 26, No. 5, pp. 308-3 13, Sept-Ott 1989. (Also AIAA paper No. 88-2541-CP, June 1988)

2. Dupuis, A.D. Proceedings of the ADPA 12th International Symposium on Ballistics, Vol. II, pp. 287-296, "Free Flight of a Dart Model With Various Surface Roughnesses," October 1990.

3. Khan, S.D., and S.K. Chung. "Effect of Geometric Variations on the Supersonic Aerodynamic Characteristics of the 75-mm XM855 APFSDS-T Projectile." ARLCD-TR-83058, U.S. Army Armament Research and Development Center, Dover, NJ, July 1984.

4. Brandon, F., and R. von Wahlde, R. "Wind Tunnel Data for Long-Rod Fin-Stabilized Projectiles," BRL-MR-3618, U.S. Army Ballistic Research Laboratory, Aberdeen Proving Ground, MD, July 1987.

5. Sigal, A. "Aerodynamic Effects of Body Roughness," AIAA paper 90-2850, 1990.

6. Fellows, K.A., and J. Carberry. "Results of Supersonic Wind Tunnel Tests on the Third Long APDS Projectile with Various Fin Designs and Buttress Threads over the Mach Number Range 2.0 to 4.9," Test Note M49/14, Aircraft Research Association, Swerby, U.K., February 1982.

7. Hendry, C.E. "Aerodynamics of Long Projectiles-Final Report, Part 2." Report No. JS 10134, British Aerospace PLC, Dynamics Group, Swerby Research Centre, Bristol, U.K., August 1984.

8. Dupuis, A.D. "Aerodynamic Characteristics of a Dart Model with Various Surface Roughness from Free-Flight Tests," DREV M-2956/89, Defence research Establishment, Valcartier, Quebec, Canada, January 1989.

9. Abate, G., W. Hathaway, and R. Whyte. "ARF-Alliant Test Program: Aerodynamic Results." (Contract No. F08635-90-C-0038), Aeroballistic Research Facility Report of Wright Laboratory, Eglin Air Force Base, prepared by Arrow Tech Associates, April 1994.

10. Babinsky, H., and J.A. Edwards. AIAA Journal of Spacecraft and Rockets, "Large Scale Roughness Influence on Turbulent Hypersonic Boundary Layers Approaching Compression Comers," Vol34. No. 1, pp. 70-75, Jan-Feb 1997.

11. Van Driest, E.R. Journal of the Aeronautical Sciences, "Turbulent Boundary Layer in Compressible Fluids," Vol. 18, No. 3, pp. 145-160, March 195 1.

12. Moore, F.G., T.C. Hymer, and R.M. McInville. "The 1995 Version of the NSWCDD Aeroprediction Code: Part II-Computer Program User's Guide and Listing." NSWCDD/TR-95/5, Naval Surface Warfare Center-Dahlgren Division, Dahlgren, VA, March 1995.

13. Forkois, J. "Cannon Caliber Electromagnetic Gun (CCEMG)." Scientific and Technical Report (Draft), CFD Chapter (Section 1.3, pp. 197 to 228), prepared by Kaman Sciences Corporation, Denver, CO, for United Defense, L.P., Corporation (under U.S Army contract No. DAAA2 1-92-C-0060), 1994.

LIST OF SYMBOLS

A_{ref} = reference area $(\pi d^2/4)$, in^2

CD = drag coefficient, drag force/$(q_\infty A_{ref})$

CL = lift coefficient, lift force/$(q_\infty A_{ref})$

CN = normal force coefficient, normal force/$(q_\infty A_{ref})$

CN_α = normal force slope coefficient, $\partial C_N/\partial \alpha$, rad^{-1}

d = projectile reference diameter, inch

G/S = grooved first body length/smooth second length

G/T = grooved first body length/threaded second length

G/G = grooved first body length/grooved second length

$K_{w(b)}$ = wing-body normal force interference modeling factor for a wing in the presence of a body

$K_{b(w)}$ = wing-body normal force interference modeling factor for a body in the presence of a wing

L = total length of the projectile, inch

l_g = length of grooved portion of the body, inch

l_{g1}, l_{g2} = lengths of grooved body portions if more than one existed, inch

M = Mach number of the projectile

N = number of fins in a fin set

p_1, p_2 = groove pitch, l/(number of grooves per inch), inch

q_∞ = dynamic pressure, $(0.5\rho V^2)$, psi

Re = flow Reynolds number per foot, ft^{-1}

R_∞ = Reynolds number based on projectile total length

V = projectile velocity, ft/s

Greek Symbols

a = body pitching angle of attack, degrees

ρ = air density, $slug/ft^3$

Subscripts

b = body alone, i.e., without fins

f = fins, tail fins or wing fins

bf = body and fins, i.e., total vehicle

fl = flare

bfl = body and flare, i.e., total vehicle

g = with body surface grooves

s = smooth body surface, i.e., without grooves

INTENTIONALLY LEFT BLANK

REPORT DOCUMENTATION PAGE

1. AGENCY USE ONLY *(Leave blank)*	2. REPORT DATE February 1999	3. REPORT TYPE AND DATES COVERED Final

4. TITLE AND SUBTITLE The Effect of Sabot Grooves on Lift Force for Kinetic Energy Projectiles	5. FUNDING NUMBERS PR: 1L162618AH80
6. AUTHOR(S) Mikhail, A.G. (ARL)	

7. PERFORMING ORGANIZATION NAME(S) AND ADDRESS(ES) U.S. Army Research Laboratory Weapons & Materials Research Directorate Aberdeen Proving Ground, MD 2 10 1 0-5066	8. PERFORMING ORGANIZATION REPORT NUMBER
9. SPONSORING/MONITORING AGENCY NAME(S) AND ADDRESS(ES) U.S. Army Research Laboratory Weapons & Materials Research Directorate Aberdeen Proving Ground, MD 21010-5066	10. SPONSORING/MONITORING AGENCY REPORT NUMBER ARL-TR-1776

II. SUPPLEMENTARY NOTES

12a. DISTRIBUTION/AVAILABILITY STATEMENT Approved for public release; distribution is unlimited.	12b. DISTRIBUTION CODE

13. ABSTRACT *(Maximum 200 words)*

The effect of grooves on the normal force of an anti-armor long rod kinetic energy (KE) projectile was analyzed and numerically quantified. The effect was studied for body alone and body with fins in which clear and distinct effects were experimentally observed for each. Wind tunnel data sets were analyzed, and algebraic, semi-empirical correlations were constructed using the main physical parameters of the projectile body and fins, as well as the flow parameters. The correlations provide a simple method of estimating the increase or decrease in the vehicle's total normal force attributable to grooves and can be implemented in fast aerodynamics design codes. One separate set of data was dedicated for independent validation, and the correlation predicted the effect reasonably well, both in magnitude and sign. The present correlation is the only one known in the literature for predicting the lift loss (or gain) attributable to grooves. In addition, a better understanding of the contributions of grooves to both body alone and fins in the presence of a body is presented. The correlation is constructed for the Mach number range of $2.0 < M < 5.5$ and for small angles of attack (less than $6°$), which cover the flight envelope of tactical KE anti-armor projectiles. The established correlations provide direct incremental lift coefficient corrections over smooth body values for useful direct design use.

14. SUBJECT TERMS aerodynamics kinetic energy projectiles grooves lift			15. NUMBER OF PAGES 55
			16. PRICE CODE
17. SECURITY CLASSIFICATION OF REPORT Unclassified	18. SECURITY CLASSIFICATION OF THIS PAGE Unclassified	19. SECURITY CLASSIFICATION OF ABSTRACT Unclassified	20. LIMITATION OF ABSTRACT